JSAE 20119203
SAE SAND2011-0913C

Smoothing HCCI Heat Release with Vaporization-Cooling-Induced Thermal Stratification using Ethanol

Magnus Sjöberg and John E. Dec
Sandia National Laboratories

ABSTRACT

Ethanol and ethanol/gasoline blends are being widely considered as alternative fuels for light-duty applications. At the same time, HCCI combustion has the potential to provide high efficiency and ultra-low exhaust emissions. However, the application of HCCI is typically limited to low and moderate loads because of unacceptably high heat-release rates (HRR) at higher fueling rates.

This work investigates the potential of lowering the HCCI HRR at high loads by using partial fuel stratification to increase the in-cylinder thermal stratification. This strategy is based on ethanol's high heat of vaporization combined with its true single-stage ignition characteristics. Using partial fuel stratification, the strong fuel-vaporization cooling produces thermal stratification due to variations in the amount of fuel vaporization in different parts of the combustion chamber. This results in a sequential autoignition event, lowering the overall combustion rate.

The amount of partial stratification was varied by adjusting the fraction of fuel injected late to produce stratification, and also by changing the timing of the late injection. The experiments show that a combination of 60 – 70% premixed charge and injection of 30 – 40 % of the fuel at 60°CA before TDC is effective for smoothing the HRR. With CA50 held fixed, this increases the burn duration by 55% and reduces the maximum pressure-rise rate by 40%. Combustion stability remains high but engine-out NO_x has to be monitored carefully. For operation with strong reduction of the peak HRR, $ISNO_x$ rises to around 0.20 g/kWh for an $IMEP_g$ of 440 kPa. The single-cylinder HCCI research engine was operated naturally aspirated without EGR at 1200 rpm, and had low residual level using a CR = 14 piston.

INTRODUCTION

The homogeneous charge compression ignition (HCCI) combustion process offers high thermal efficiency and very low nitrogen-oxide (NO_x) and particulate emissions. Therefore, HCCI combustion is one available option for improving the efficiency of the spark-ignited gasoline engine. HCCI-type combustion is also being implemented in the latest generation of compression-ignited diesel engines in order to reduce the requirement for NO_x aftertreatment. However, several technical hurdles need to be overcome before HCCI combustion will see broad application. Maintaining an acceptable pressure-rise rate (PRR) to avoid knocking at high loads is one important research area. One effective way to reduce the PRR is to retard the combustion phasing [1,2]. However, the amount of combustion-phasing retard that can be applied while maintaining high combustion stability varies with fuel type [3]. Specifically, combinations of fuel type and operation strategy that render strong early heat release just prior to the main combustion allow more combustion-phasing retard [4].

Since petroleum is a limited resource, at present there is great interest in developing alternative fuels. Worldwide, the most widespread alternative fuel for light-duty engines is currently ethanol. Practically all gasoline SI engines tolerate some fraction of ethanol in the fuel (~10%), and most SI engines are readily adapted for operation on fuels that contain up to 85% ethanol (*i.e*. flex-fuel engines) [5]. Based on the importance of ethanol as an alternative fuel and the current trend towards more advanced and efficient engines, it is important to fully understand the characteristics of ethanol when used in advanced combustion systems for internal combustion engines. Consequently, a recent comprehensive HCCI study was conducted by the current authors to map out the autoignition characteristics of ethanol [6]. One of the fundamental findings was that neat ethanol is a true single-stage ignition fuel with very little early heat release prior to the onset of main combustion, regardless of engine speed and intake pressure boost.

Because ethanol is a true single-stage ignition fuel with very little early heat release, the amount of combustion-phasing retard that can be applied while maintaining stable combustion is less than for other fuels. Therefore, ethanol offers less potential for applying combustion-phasing retard to increase power output in HCCI engines than does gasoline [4,6]. This fact has to be considered in the light of expected higher availability of ethanol as a motor fuel [7], both as E85 and intermediate blends (*e.g.* E15 – E30). However, with a change of fuel composition, several other important factors change simultaneously. For example, both the stoichiometric air/fuel-ratio (AFR_{st}) and latent heat of vaporization differ considerably between gasoline and ethanol. As a result, for a given engine load, the vaporization-cooling potential is more than four times greater for ethanol. For a combustion system like HCCI, compensation must be provided for this additional cooling to ensure robust autoignition and combustion. On the other hand, this strong vaporization cooling can potentially be exploited to change the in-cylinder thermal field. This may be a very important consideration, since for classical HCCI, the combustion rate is controlled by the sequential autoignition from hotter to colder in-cylinder zones [8].

SCOPE AND OBJECTIVES

Fuel stratification has the potential to create thermal stratification due to uneven vaporization cooling. If the naturally occurring thermal stratification due to heat transfer can be enhanced, this should lead to longer burn duration. Compared to conventional fuels, ethanol has a high latent heat of vaporization and strong cooling potential. Based on this, the primary objective of this study is to experimentally examine the use of direct injection of ethanol to create fuel stratification and achieve a longer HCCI combustion event with reduced peak HRR. For better understanding of the in-cylinder processes, some of ethanol's autoignition and thermodynamic characteristics are examined in detail. To put the results in context, comparisons are made with previously published data for other fuels at similar operating conditions. In addition, using previous data for iso-octane, some of the engine's characteristics regarding both fuel stratification and the naturally occurring thermal stratification due to heat transfer are discussed.

First, the experimental setup, data acquisition and analysis are described. This is followed by a description of the chemical-kinetics mechanism and the model setup. The results are then divided into five main parts:

1. Review of ethanol's distinct single-stage autoignition characteristics and the sensitivity of the autoignition timing to changes of the charge temperature in comparison with data for other fuels.
2. Fundamental investigation of the sensitivity of the autoignition timing to changes of the fuel/air-equivalence ratio (ϕ-sensitivity) for gas phase only.
3. Quantification of experimentally attainable vaporization cooling using direct injection of liquid ethanol (in comparison with iso-octane), and the influence of vaporization cooling on the ϕ-sensitivity of ethanol.
4. Discussion of ways to achieve vaporization-cooling-induced thermal stratification and its relationship to the naturally occurring thermal stratification caused by normal wall heat transfer.
5. Demonstration of the use of partial fuel stratification with ethanol to achieve an enhanced thermal stratification with lower peak combustion rates.

Finally, a summarizing comparison is made between this application of partial fuel stratification using ethanol and previously published applications of partial fuel stratification using other types of fuels.

EXPERIMENTAL SETUP

The engine used for this study is based on a Cummins B-series diesel engine, which is a typical medium-duty diesel engine with a displacement of 0.98 liters/cylinder. A schematic of the setup is shown in Fig. 1. The configuration of the engine and facility is the same as for recent studies (*e.g.* Refs. [4,6]).

Furthermore, the schematic in Fig. 1 shows that the piston used for the current experiments with ethanol provides an open combustion chamber with a large squish clearance and a quasi-hemispherical bowl. The geometry renders a geometric compression ratio (CR) of 14:1. The bowl of this piston is deeper than the shallow scallop design used in several previous publications (*e.g*. Ref. [3]). However, tests show that the engine performance is nearly identical. Nonetheless, it can be noted that the data for fuels other than ethanol that are presented here (but previously published) were acquired with pistons that have more shallow piston bowls. In the case of optical data, flat-top pistons were used.

To achieve partial fuel stratification, a combination of premixed and direct injection (DI) fueling was used. The premixed fueling system, shown at the top of the schematic in Fig. 1, consists of a GDI injector mounted in an electrically heated fuel-vaporization chamber and appropriate plumbing to ensure thorough premixing with the air upstream of the intake plenum. The DI fueling is accomplished using a second GDI injector mounted centrally in the cylinder head. For the current tests with ethanol, an 8-hole Bosch injector was used at a fuel pressure of 120 bar. The included angle was 70°. A positive-displacement fuel-flow meter was used to determine the amount of fuel supplied. The intake air was metered with a sonic nozzle. A main air heater and tank heaters (not shown) were used to preheat the mixture of air and fuel. An auxiliary air heater mounted close to the engine was used to precisely control the intake temperature of the inducted charge. Intake temperatures were monitored using thermocouples mounted in the two intake ports close to the cylinder head. Intake pressure (P_{in}) was measured with a

TABLE 1. Engine Specifications

Displacement (single-cylinder)	0.981 liters
Bore	102 mm
Stroke	120 mm
Connecting Rod Length	192 mm
Nominal Geometric Compression Ratio	14:1
No. of Valves	4
IVO	0°CA*
IVC	202°CA*
EVO	482°CA*
EVC	8°CA*
Intake Air Swirl Ratio, Both Ports Combined	0.9

* Valve closing and opening timings refer to 0.1 mm lift.

pressure transducer mounted on the intake runner. The reported absolute P_{in} values are crank-angle averaged over 200 cycles. Engine specifications are listed in Table 1. A detailed description of the engine modifications for HCCI operation can be found in Ref. [9].

Cylinder pressure measurements were made with a transducer (AVL QC33C) mounted in the cylinder head approximately 42 mm off center. The pressure transducer signals were digitized and recorded at ¼° crank angle (CA) increments for typically 200 consecutive cycles per operating point. To compute the maximum pressure-rise rate (PRR_{max}) for an operating point, each individual cycle is first low-pass filtered (< 2.5 kHz) and then analyzed with a linear fit over a moving ±0.5°CA window to extract the PRR_{max} of that cycle. The reported PRR_{max} associated with an operating point is then computed by averaging all PRR_{max} values of the 200 individual cycles. Similarly, the 50% burn point (CA50) was first computed from the low-pass-filtered pressure trace for each individual cycle (without heat-transfer correction), and then averaged.

A second method of computing the heat-release rate was used for the presented HRR traces. Here, the heat-release rate was computed in a more refined way from the pressure trace (with the 2.5 kHz low-pass filter applied), using the Woschni correlation for heat transfer [10].

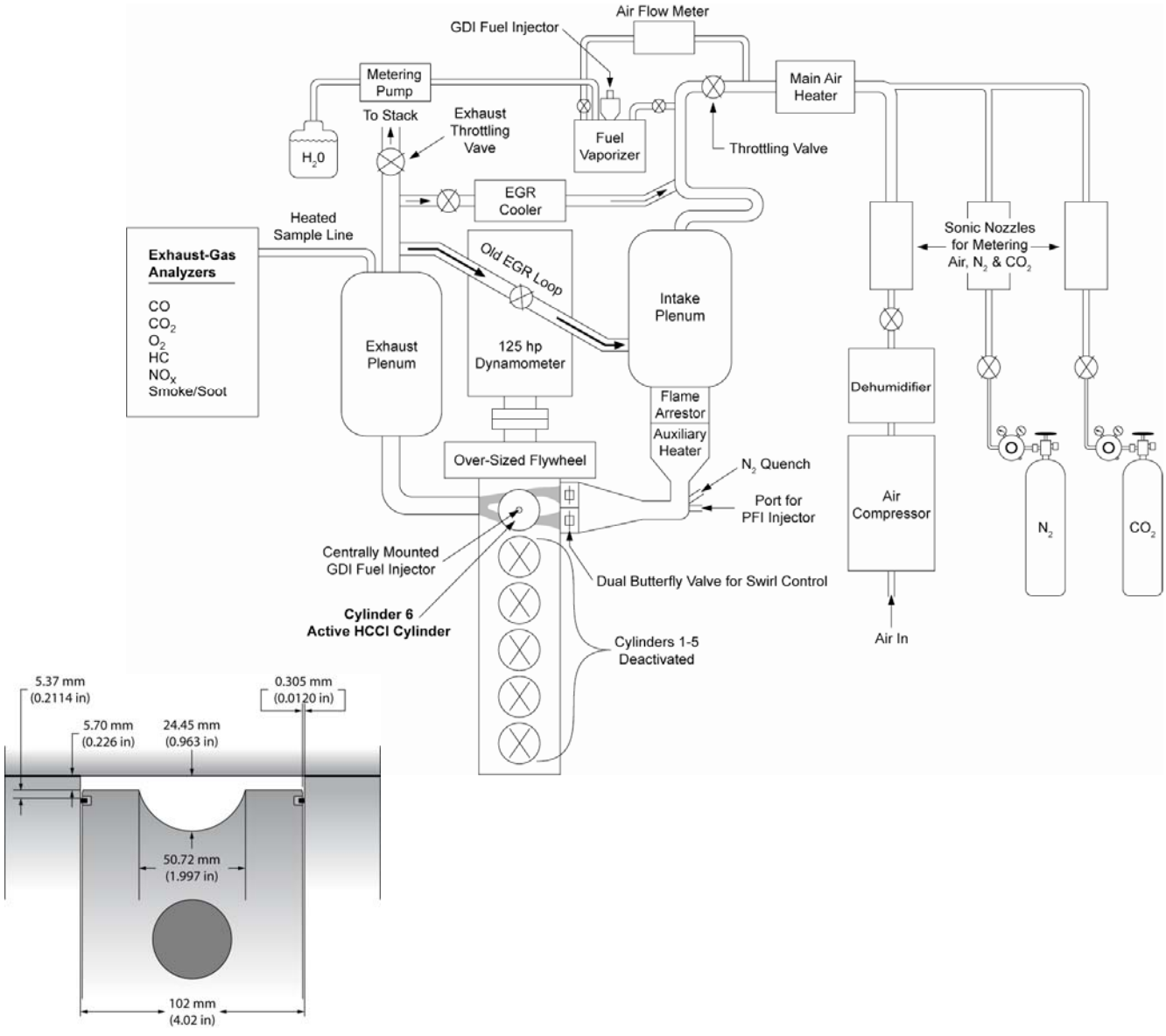

Figure 1. Schematic of the HCCI engine facility, and combustion-chamber dimensions at TDC with the CR = 14 piston.

Charge temperatures during the closed part of the cycle (*i.e.* compression/expansion) are computed using the ideal-gas law in combination with the measured pressure (ensemble-averaged over 200 cycles), the known cylinder volume, and the trapped mass. The trapped mass equals the sum of the supplied air, fuel, and residuals. The residual mass is computed by applying the ideal-gas law to the clearance volume at TDC-valve-overlap, using a pressure that was determined from cycle-simulation modeling (using Ricardo's WAVE program) and an iteratively estimated residual temperature based on exhaust-blowdown cooling to this pressure. The average molecular weight used to calculate the charge temperature during the compression stroke corresponds to that of the trapped gases - including fresh air, retained residuals, and fuel. During the combustion event, and in proportion to the mass fraction burned, the average molecular weight in the calculations is gradually changed to that of the measured exhaust composition. This exhaust molecular weight is then used for the remainder of the expansion stroke and for computing the trapped residual mass.

Exhaust emissions data were also acquired, with the sample being drawn from just downstream of the exhaust plenum using a heated sample line. For all conditions, the levels of CO, CO_2, HC, NO_X, O_2 were measured using standard exhaust-gas analysis equipment, as shown in Table 2. Since the ethanol fuel is oxygenated, a separate test was performed to check the response of the HFID to ethanol. It was found that the carbon-atom-detection efficiency was 65%. Accordingly, the HC emissions reported here have been multiplied by 1.53 to correct for this, with the assumption that the HFID readout during engine operation is dominated by unburned fuel (*i.e.* ethanol molecules) in the exhaust [11]. Smoke measurements were also made with an automated smoke meter, but no soot emissions were detected.

TABLE 2. Emissions Analysis Equipment

CO	Non-Dispersive Infrared Detector, Rosemount 880A
CO_2	Non-Dispersive Infrared Detector, CAI 602 NDIR
HC	Heated Flame Ionization Detector, CAI 600 HFID
NOX	Chemiluminescence Analyzer, Rosemount 951A
O2	Paramagnetic Analyzer, Rosemount 755R
Smoke	Optical-Density of Filter Paper, AVL415S

Because HCCI combustion is very sensitive to temperature, the engine coolant and oil were both preheated to 100°C before starting the experiments. For all data presented, 0°CA is defined as TDC intake (so TDC compression is at 360°). This eliminates the need to use negative crank angles or combined bTDC, aTDC notation.

The main fuel used for this study is neat (100%) ethanol, and this fuel was used for all operation with partial fuel stratification. In addition, 190-proof ethanol (95% ethanol, 5% water by volume), and neat iso-octane were used for the separate vaporization-cooling measurements. All of these fuels are fairly volatile, and this facilitates the charge preparation process. Table 3 shows selected fuel data for ethanol and iso-octane. In the first results section, the autoignition characteristics of ethanol are compared with iso-octane, gasoline, and two PRF blends. The properties of the three latter fuels can be found in previous work [6,12].

TABLE 3. Fuel Properties

Fuel:	**100% Ethanol**	**100% Iso-Octane**
RON	107	100
MON	89	100
Antiknock Index (RON+MON)/2	98	100
C-atoms	2	8
H-atoms	6	18
O-atoms	1	0
Molecular Weight [g/mole]	46.07	114.2
A/F-Stoichiometric [kg air/ kg fuel]	9.00	15.13
Specific Heat Capacity - C_p [J/g·K] @ 700K	2.58	3.26
Heat of Vaporization [MJ/kg] @ 298 K	0.84	0.31
Lower Heating Value for Gas-phase Fuel [MJ/kg fuel]	27.75	44.65
Lower Heating Value for Stoichiometric Charge [MJ/kg]	2.775	2.769

CHEMICAL-KINETICS MODELING SETUP

The chemical-kinetic modeling approach used in this work is identical to one used recently by the authors [6,12]. The calculations were carried out using a special multi-zone version of the Senkin application of CHEMKIN III developed at Sandia [13,14]. The model treats each zone as a single lumped mass with uniform composition and thermodynamic properties. The chemistry is treated independently for each zone. The only coupling between zones is the pressure, which is assumed to equilibrate instantaneously as heat is released in any of the zones. The total volume of all zones is modeled according to the standard slider-crank relationship [10], using the geometry and specifications of the Sandia HCCI research engine shown in Table 1. As a result, the volume of each zone effectively depends on its mass and temperature relative to the other zones. In the current study, 11 zones were used and the thermal distribution across the zones is described in Appendix A.

A newly developed reaction mechanism for ethanol was used [15]. The ethanol mechanism has 58 species and 310 reactions, and it has been validated against experimental flow-reactor and shock-tube data. It is developed to be an integrated part of a gasoline surrogate mechanism [16]. This much larger surrogate mechanism is a joint effort between the National University of Ireland (NUI) – Galway (Curran, Serinyel, and Metcalfe) and Lawrence-Livermore National Lab (LLNL) (Pitz and Mehl). Additionally, as a part of a collaboration between Sandia and the University of New South Wales (UNSW) in Australia, two other mechanisms that are available in the open literature, Refs. [17,18], were examined [19]. However, neither of these ethanol mechanisms had sufficient reactivity so they required unrealistically high charge temperature to reproduce the experimental combustion phasing, therefore they were not used in this work.

For simplicity, heat transfer effects were not modeled. However, to ensure a charge-pressure history during the compression stroke that is very similar to that of the experiment, the model was set up with CR = 12.8. This is somewhat lower than the experimental CR = 14. The air was modeled using the correct proportions of N_2, O_2 and CO_2, where atmospheric argon was lumped with atmospheric N_2. The residuals were modeled using CO_2, H_2O, N_2, CO, unburned fuel, and air. It should be noted that the amount of residuals was low as a result of the use of conventional valve timings. For operation using ethanol, the residual mass fraction was around 4.2%.

RESULTS

The engine speed was kept at 1200 rpm throughout this study. Unless noted, the intake pressure (P_{in}) was set to = 100 kPa, simulating naturally aspirated operation.

EARLY AUTOIGNITION HEAT RELEASE

The successful use of vaporization cooling to enhance the in-cylinder thermal stratification and in this way achieve an extended burn duration requires selection of a suitable fuel. As mentioned in the Introduction, the fact that ethanol has a much smaller amount of heat release prior to the main combustion is a characteristic feature that distinguishes ethanol from other common fuels. As will be shown, this characteristic feature of ethanol is very important for the use of vaporization cooling to smooth HCCI heat release. Thus, this section compares the early heat release of ethanol with that of several other fuels.

Figure 2 plots the heat release just prior to onset of the main combustion for ethanol and four other fuels. From here forward, the heat-release rate just prior to the main combustion will be called intermediate-temperature heat-release rate (ITHRR) in accordance with the terminology used in previous works [20]. The low-octane PRF blends stand out with high ITHRR. This stems partly from the low-temperature combustion (which occurs in the 338-350°CA range, outside the plot area) of these PRF blends, which creates a large number of reactive fuel fragments [20]. Conversely, the CHEMKIN model predicts that the ethanol molecule is stable up to a temperature of approximately 960K. Consequently, Fig. 2a shows that ethanol does not start to break down until roughly 10°CA prior to hot ignition. The timing of the hot ignition is indicated by the rapid rise in HRR around 364°CA. As a result, ethanol exhibits a very low ITHRR prior to hot ignition. Iso-octane and gasoline also show low ITHRR for these operation conditions, albeit not quite as low as ethanol. As a side note, Fig. 2a shows that significant amounts of both acetaldehyde and formaldehyde are formed during the autoignition process of ethanol. Aldehydes are known to influence the autoignition timing [3,21,22], but these intermediate species are probably not very important for combustion-phasing control of this low-residual engine as long the combustion efficiency remains high. However, they may be of greater importance for high-residual engines, in particular if significant amounts remain unburned and participate in the next cycle.

It can be noted that the predicted ITHRR in Fig. 2a is very similar to the experimental curve for ethanol, providing confidence in the multi-zone modeling approach. Also, the bottom-dead-center temperature (T_{bdc}) required to match the 10% burn point (CA10) of the model to the experimental CA10 is less than 1°C different from the experimental value of 154°C.

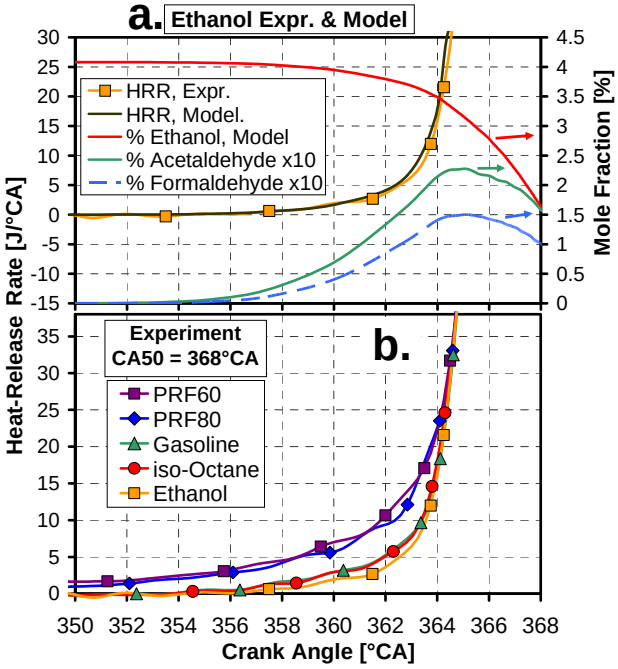

Figure 2. ϕ = 0.40. a) Ethanol experimental and model ITHRR, and model prediction of ethanol breakdown, acetaldehyde and formaldehyde formation. b) Comparison of the ITHRR for five fuels. For ease of interpretation, non-ethanol curves shifted slightly (0.2 – 1.2°CA) to the left to make the curves cross at 364.8°CA. Modified from Ref. [12].

THERMAL SENSITIVITY OF AUTOIGNITION TIMING

Figure 3 shows how T_{in} has to be adjusted to achieve a certain CA10 for ethanol, iso-octane and PRF80. Both ethanol and iso-octane exhibit single-stage ignition behavior without low-temperature heat release (LTHR). As a result, their T_{in} requirements are comparable. Even so, Fig. 3a shows that iso-octane requires between 34 and 41°C higher T_{in} than ethanol for this range of CA10. This shows that ethanol has a higher autoignition reactivity than iso-octane under these conditions (1200 rpm and P_{in} = 100 kPa). This higher reactivity is in agreement with the lower MON of ethanol, as Table 3 shows. (MON numbers are acquired at 900 rpm with high T_{in}, so they are more relevant for this comparison since RON numbers are acquired at 600 rpm and low T_{in}. [6]) In contrast to ethanol and iso-octane, PRF80 requires a much lower T_{in}, so it is plotted separately in Fig. 3b. Under these operating conditions, PRF80 exhibits LTHR, and this explains why its T_{in} has to be low.

Not only are the T_{in} requirements different between the fuels, the slope of the curves in Fig. 3 are different as well. PRF80 has the steepest slope, so among these fuels its combustion phasing has the lowest sensitivity to changes of T_{in}. Its low T_{in} sensitivity can be explained by its LTHR in combination with enhanced ITHR [3]. The presence of LTHR reduces the sensitivity of the autoignition timing to changes of the charge temperature because the amount of LTHR increases with decreasing T_{in}, thus counteracting the direct influence of changes in T_{in} on the charge temperature at TDC. The enhanced ITHR in the 350 - 363°CA range (see Fig. 2b) increases the temperature-rise rate (TRR) just before the hot-ignition point. As explained in detail in [3], with a higher TRR, the timing of transition into hot ignition becomes less sensitive to changes of the charge temperature. Consequently, the higher TRR due to enhanced ITHR contributes to the low T_{in} sensitivity for PRF80 (Fig. 3b).

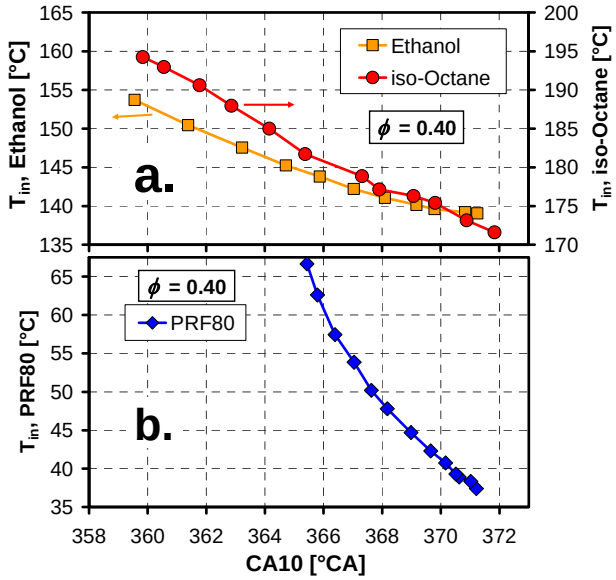

Figure 3. Required T_{in} as a function of CA10 for ethanol, iso-octane, and PRF80. ϕ = 0.40.

In contrast, Fig. 3a shows that the CA10 of both ethanol and iso-octane are much more sensitive to changes of T_{in}. Neither ethanol nor iso-octane exhibit LTHR, and Fig. 2b shows much less ITHR for these fuels. Consequently, the TRR prior to hot ignition is also much lower, and this explains the higher T_{in} sensitivity. Examination of Fig. 3a reveals that ethanol has a slightly higher T_{in} sensitivity than iso-octane. This is consistent with the somewhat lower ITHR and TRR prior to the hot ignition. In this sense, ethanol is a more pronounced single-stage-ignition fuel than iso-octane.

ϕ- SENSITIVITY OF ETHANOL

With this understanding of ethanol's high thermal sensitivity, the influence on ethanol's autoignition by changes to the fuel concentration is investigated. Gas-phase effects are first examined before vaporization-cooling effects are considered. However, with the existing experimental hardware, the required gas-phase-only data cannot be conveniently generated using fully premixed fueling. This is the case because as the amount of fuel is adjusted to change ϕ in a continuously firing engine, the charge temperature at BDC (T_{bdc}) also changes despite T_{in} being held constant. These changes of T_{bdc} occur because the varying amounts of fuel burned affect both in-cylinder wall temperatures (T_{wall}) and residual gas temperatures ($T_{residuals}$) [6]. It would be difficult and time consuming to try to compensate for this by adjusting both T_{in} and the coolant temperature to achieve constant T_{bdc} and T_{wall}. Additionally, $T_{residuals}$ would still change with ϕ. Instead of trying to use experiments to generate the desired gas-phase data, the model was set up to simulate fully premixed operation with constant T_{bdc}. Please note that the model was extensively compared with engine results in Ref. [6], and generally good agreement was found. In particular, the model response to changes of ϕ agreed fairly well with the experiment. Figure 4 shows the model response to changes of the supplied ϕ when T_{bdc} is held constant. The results are insightful. With increasing ϕ, the autoignition timing is retarded.

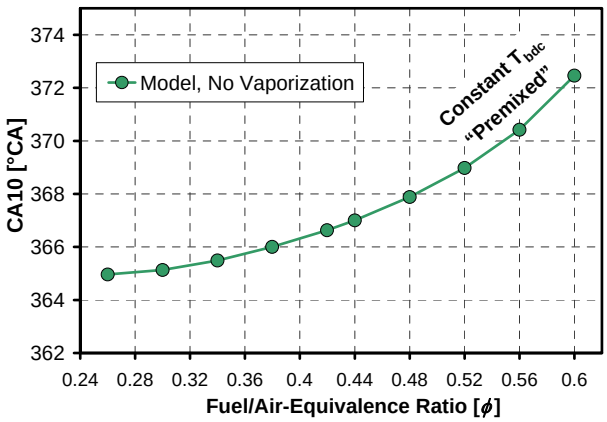

Figure 4. Model prediction of premixed engine operation. CA10 is plotted against ϕ for constant $T_{bdc,max}$ = 152°C (see Appendix A for definition of $T_{bdc,max}$). Only gas-phase ethanol. Reproduced from Ref. [6].

To provide insights into why the autoignition of ethanol is retarded with increasing ϕ, Fig. 5 plots the temperature traces for ϕ = 0.30 and 0.60. As can be seen, the compressed-gas temperature 5°CA before TDC is 47 K lower for the higher-ϕ case. This is a thermodynamic effect caused by a higher heat-capacity of the charge, leading to a lower ratio of specific heat capacities (lower γ). This is a well-known cooling effect that is used regularly to suppress engine knock at high loads in SI gasoline engines by operating the engine rich of stoichiometric [23].

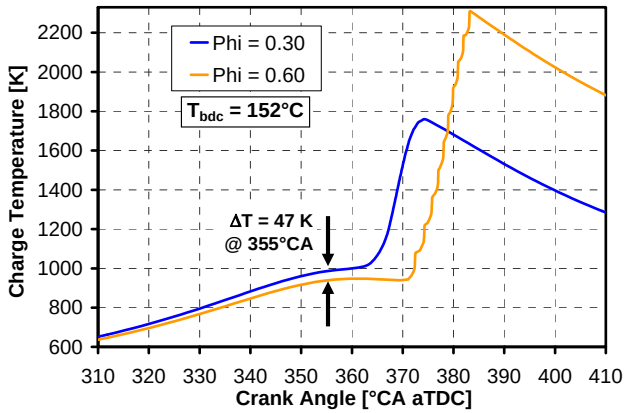

Figure 5. Model prediction of temperature traces for operation with $T_{bdc,max}$ = const = 152°C with ϕ = 0.30 and 0.60. Ethanol, 1200 rpm, and P_{in} = 100 kPa. Reproduced from Ref. [6].

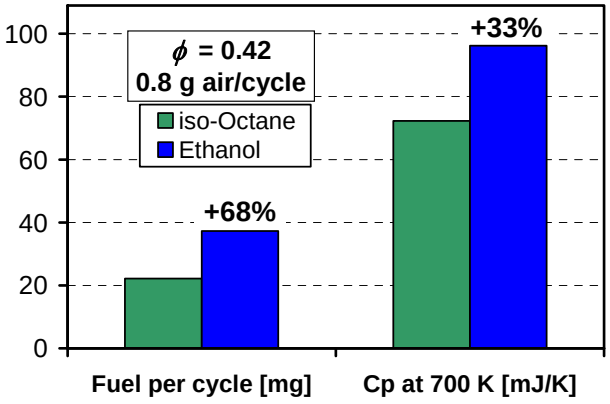

Figure 6. Illustration of differences in fueling rate and heat capacity of the fuel between iso-octane and ethanol. Reproduced from Ref. [6].

However, the autoignition-suppression effect resulting from gas-phase thermodynamic cooling is greater for ethanol than for traditional non-oxygenated fuels like gasoline. (In the following example, iso-octane serves as a gasoline surrogate since its thermodynamic properties are more accurately known.) First, the stoichiometric air/fuel ratio is 40.5% lower for ethanol; 9.0 vs. 15.1 for iso-octane. As Fig. 6 shows, this requires 68% more fuel mass to be supplied to achieve the same ϕ. With the same ϕ, the delivered chemical energy is practically the same since also the lower heating value of ethanol is 40.5% lower than that of iso-octane. Ethanol has substantially lower mass-specific heat capacity than iso-octane [6,24]. Nonetheless, because the required amount of fuel is 68% greater, the total heat capacity of the fuel in gas phase becomes 33% higher than for iso-octane. (The heat capacities of the two fuels were computed for a temperature of 700 K, which is roughly half-way between T_{bdc} and the ignition temperature.) This fact, combined with the high temperature sensitivity of ethanol autoignition (see Fig. 3a), explains why Fig. 4 shows such a strong retarding effect of increasing ϕ.

To better understand the fuel-chemistry contribution to the gas-phase ϕ-sensitivity plotted in Fig. 4, additional computations were performed. First, the model was exercised with all the reactions disabled. This allowed the determination of the T_{bdc} adjustment required to compensate for the increase of heat capacity with ϕ and achieve the same temperature at 355°CA. Figure 7a shows how $T_{bdc,max}$ had to be adjusted to achieve a constant compressed-gas temperature at 355°CA, which is when significant breakdown of ethanol starts according to Fig. 2a. (See Appendix A for definition of $T_{bdc,max}$.) With the cooling effect of more gas-phase ethanol removed, the CA10 trend reverses, as plotted in Fig. 7b and illustrated by the curved arrow. With thermodynamic effects removed, cases with higher ϕ ignite earlier, indicating that there is a small direct effect of the fuel concentration on the rate of the autoignition reactions.

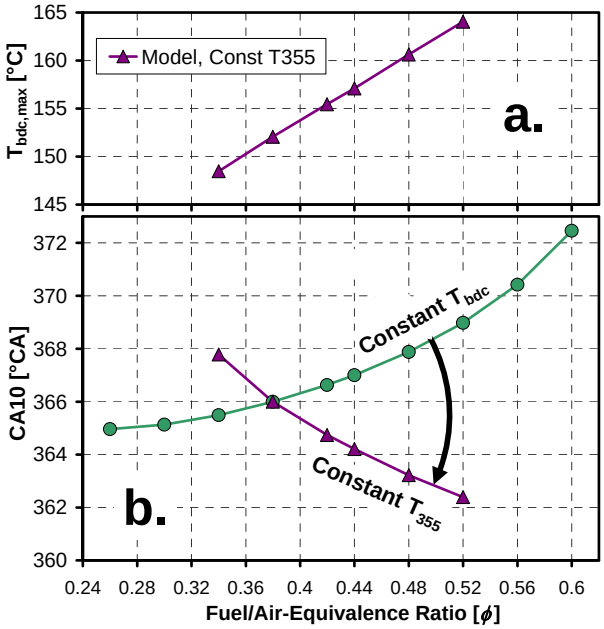

Figure 7. Effect of removal of γ-effect on ϕ-sensitivity. Gas-phase only. Ethanol, 1200 rpm and P_{in} = 100 kPa.

Figure 8 illustrates the fuel-chemistry effects by plotting the temperature and heat-release traces for two different ϕ, using the $T_{bdc,max}$ from Fig. 7. For each ϕ, the compressed-gas temperatures are identical until 353°CA regardless of the reactions being activated in the model or not. However, beyond 355°CA, the effect of the heat release can been seen as the temperature traces rise above the respective "no reaction" temperature trace for each ϕ. Furthermore, it can been seen that the higher-ϕ case rises more quickly above its "no reaction" trace. This happens because the HRR around 355°CA is more

than twice as large for the higher-ϕ case, as shown in Fig. 8b. Thus, the ITHRR scales with the fuel concentration, despite the single-stage ignition characteristics of ethanol. Without this chemistry effect, the slope of the Constant T_{bdc} curves in Figs. 4 and 7 would have been even steeper (i.e. even more retard with high ϕ).

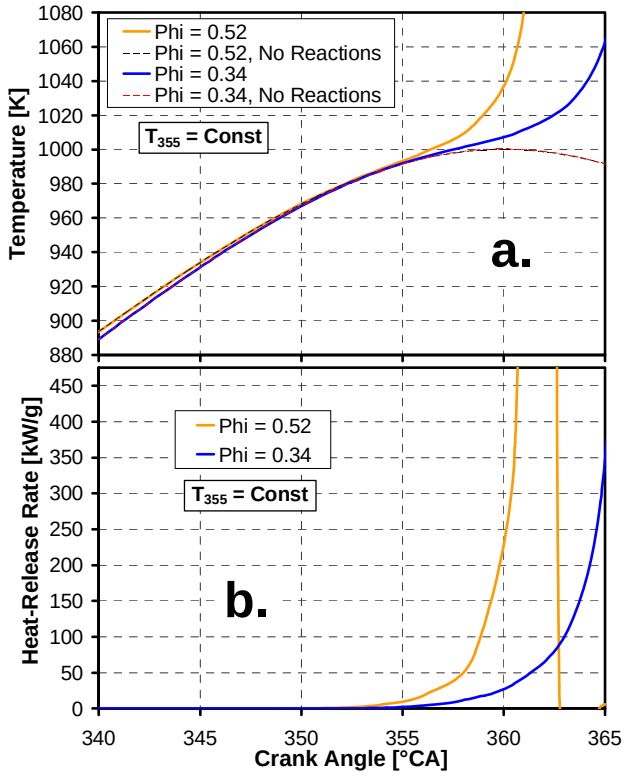

Figure 8. Model prediction of operation with T_{bdc} adjusted to provide equal temperature at 355°CA for ϕ = 0.34 and 0.52. Ethanol.

QUANTIFICATION OF VAPORIZATION COOLING

With this background of gas-phase effects, the influence of vaporization cooling can be better understood. In this section, the magnitude of the vaporization cooling that can be achieved experimentally will be compared with theory. At the time that these particular measurements were performed, only 190-proof ethanol was available. However, this is a rational fuel to examine because this 95%/5% alcohol/water blend is available as a motor fuel in some markets. In addition, it is cheaper and less energy consuming to produce than water-free (dehydrated) ethanol [25]. Figure 9 compares some of the characteristics related to vaporization cooling for 190-proof ethanol and iso-octane (as a gasoline surrogate).

To maintain constant ϕ, 79% more 190-proof ethanol has to be injected, as shown in Fig. 9. This increase in required fuel mass is greater than for pure ethanol (Fig. 6) simply because the water does not contribute any heating value to the fuel. On a mass basis, the latent heat of vaporization is about 200% higher for 190-proof ethanol. In combination with the higher required fuel mass, the potential cooling with 190-proof ethanol is approximately 440% higher than for iso-octane.

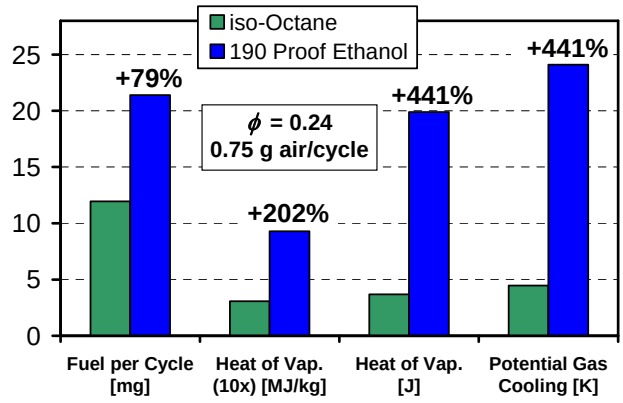

Figure 9. Illustration of differences in fueling rate and vaporization cooling between iso-octane and 190-proof ethanol.

To examine if this strong cooling can be achieved in practice, the engine was carefully operated with ϕ = 0.24 as described below. First, the effects of fuel vaporization on the charge temperature were eliminated by the use of the external electrically heated fuel vaporizer. T_{in} was held constant for each fuel. T_{in} = 195°C was used for 190-proof ethanol and a lower T_{in} = 144°C for iso-octane, for which a CR = 18 piston was installed at the time of the iso-octane tests [26]. These T_{in} settings rendered combustion phasing near TDC for both fuels. The engine was kept in this premixed firing mode for 20 minutes to assure that both the engine and the intake system had come to thermal equilibrium. At this point, without changing the settings on the intake air heaters or the mass flow of air metered by the sonic orifice, the premixed fueling was turned off, and instead the fuel was injected directly into the cylinder. For the current ethanol study a multi-hole injector was used, and the previously acquired iso-octane data used a hollow-cone injector [26]. The start of injection was initially set very early, 20°CA, to obtain substantial spray impingement onto the piston without losing fuel to the exhaust ports, which nominally close at 8°CA. Then, the start of injection was moved progressively later while the changes in intake pressure, combustion phasing, and other parameters were recorded. The injection timing sweep ended at 200 -210°CA, which is near intake valve closing (IVC). After these last DI data points, the fueling was switched back to premixed fueling. Both the manifold pressure and combustion phasing returned very close to the starting point, thus indicating that the intake system had been thermally stable during the injection-timing sweep. Some results from this operation are shown in Fig. 10.

Figure 10 shows the influence of injection timing on the BDC temperature. The plotted BDC temperature is not a direct measurement. Rather it is computed from changes of the volumetric efficiency of the engine, following the methodology presented in Ref. [27]. Figure 10 shows that all data points for DI fueling have a BDC temperature that is lower than for fully premixed fueling, indicating various degrees of vaporization cooling. The amount of cooling is highly dependent on both the fuel type and the injection timing. For early injection, the fuel sprays interact

more with the piston top and significant amount of the vaporization heat comes from the piston, as also argued by Anderson *et al.* [28]. For both fuels, the strongest cooling occurs for start of injection (SOI) around 120 – 140°CA. For these SOIs, the temperature drop relative premixed operation is very similar to the theoretical predictions (Fig. 9), as the annotations in Fig. 10 show. This experimentally demonstrates that indeed the magnitude of cooling by vaporization is 4 – 5 times greater for 190-proof ethanol compared to iso-octane. Since pure ethanol is used in the following sections, it should be noted that the vaporization-cooling effect will be somewhat smaller. Calculations indicate a cooling effect of pure ethanol that is 15% weaker than for 190-proof ethanol, and 360% stronger than for iso-octane.

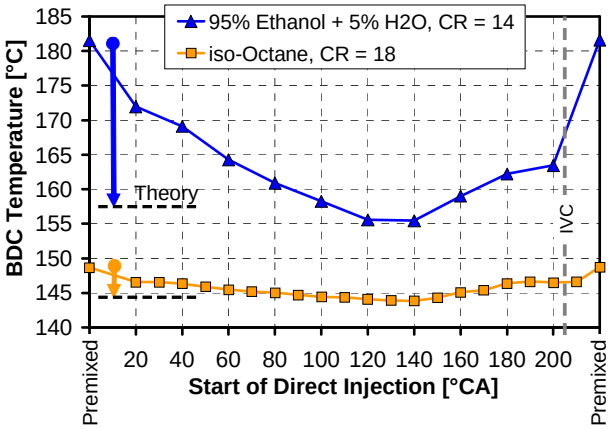

Figure 10. BDC temperature as a function of injection timing for 190-proof ethanol (T_{in} = 195°C, CR = 14) and iso-octane (T_{in} = 144°C, CR = 18). ϕ = 0.24 and 1200 rpm.

Furthermore, Fig. 10 shows that the apparent cooling is reduced when the injection is retarded in the 140 - 200°CA range. This is not an actual reduction of the charge cooling, rather it reflects the fact that the vaporization of fuel cannot fully influence the cylinder-fill process when the fuel is injected only shortly before IVC. Since the methodology used to estimate T_{bdc} is based on detecting changes to the volumetric efficiency [27], it appears like less cooling is occurring for SOI > 140°CA.

With this knowledge of the vaporization potential, the influence of direct injection on the ϕ-sensitivity of ethanol is examined. However, when the fueling rate is changed for normal continuously fired operation (premixed or DI), both the wall and the residual temperatures change. In turn, these temperature changes can dominate any observed changes of the combustion phasing. To isolate the combined effects on the combustion phasing of changes of vaporization cooling, γ, and fuel-chemistry with adjustment of ϕ, an alternately fired mode was used [26]. In this mode, the engine is fired for 19 cycles at base-ϕ = 0.42 and then for the 20th cycle at a variable ϕ, with the sequence repeating every 20th cycle. This alternately fired mode, designated as fire 19/1, is illustrated in Fig. 11. Data were acquired only on the 20th cycle of each sequence for 40 successive sequences.

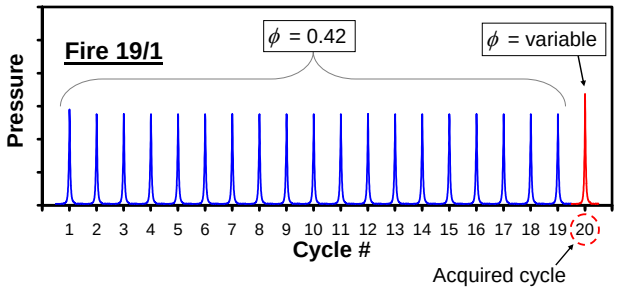

Figure 11. Illustration of the alternate-fire operational mode - fire 19/1.

Figure 12 shows the result using the fire 19/1 technique in comparison with the model result for premixed fueling. It can be seen that the vaporization cooling considerably increases the sensitivity of CA10 to changes of ϕ. The corresponding pressure and HRR traces are plotted in Fig. 13. The effect is strong because the combined effect of increased vaporization cooling and reduced γ with higher ϕ completely dominates the slightly enhanced autoignition chemistry.

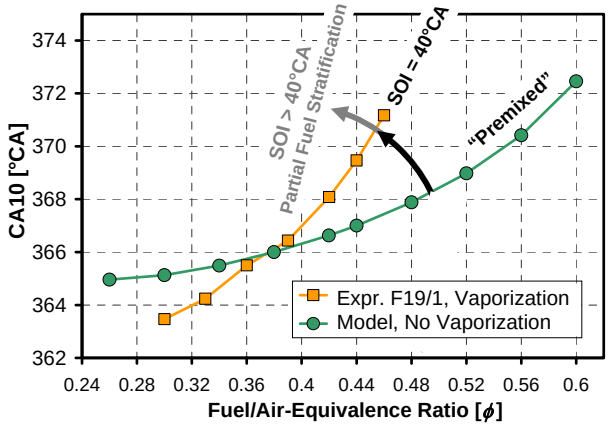

Figure 12. Effect of vaporization cooling on ϕ-sensitivity, determined using the fire 19/1 mode with SOI = 40°CA. Experiment is using 100% ethanol with T_{in} = constant = 150°C. Model has constant $T_{bdc,max}$ = 152°C and with all fuel being in gas phase to simulate fully premixed operation.

It should be noted that these results are for an SOI of 40°CA. This early injection timing was chosen since earlier studies have indicated that the charge is most well mixed for this SOI. A well-mixed charge was desirable for these tests in order to not introduce effects of fuel stratification on the measured ϕ-sensitivity. However, Fig. 10 shows that the vaporization-cooling effect for SOI = 40°CA is slightly less than half compared to SOI = 140°CA. Therefore, the SOI = 40°CA data in Fig. 12 most likely underestimate the ϕ-sensitivity of ethanol for operation with partial fuel stratification, since such operation uses injection during the compression stroke where a majority of the heat for vaporization is expected to come from the in-cylinder air (like SOI = 140°CA in Fig. 10). The expectation for higher effective ϕ-sensitivity is illustrated by the gray curved arrow and annotation in Fig. 12, but it is uncertain

exactly what the ϕ-sensitivity is for operation with partial fuel stratification.

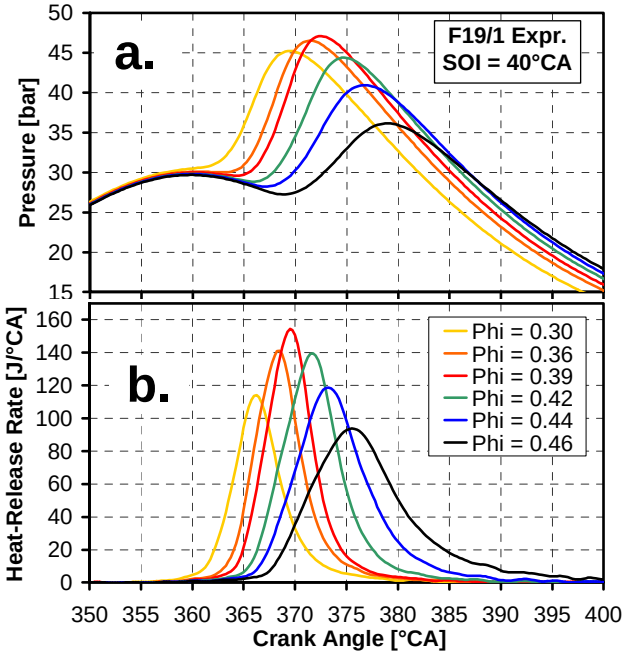

Figure 13. (a) Pressure and (b) HRR traces that illustrate the combustion-phasing retard for higher ϕ caused by increased vaporization cooling with increased DI fueling. Ethanol.

STRATIFICATION FOR STAGED COMBUSTION

The results in Fig. 12 and 13 are intriguing since they suggest that it should be possible to achieve a highly staged combustion event by using appropriate fuel stratification to produce a range of ϕ in the combustion chamber. This section discusses the rationale for using *partial* fuel stratification. The complexities of the interacting fuel and thermal fields are also highlighted.

The widest possible temperature range due to vaporization cooling would be achieved by stratifying the charge so that the local equivalence ratios range from zero (air only) to the highest permissible ϕ. However, this is not a desirable stratification for two reasons. First, any in-cylinder regions with near zero fuel concentration would not contribute to the $IMEP_g$, thereby lowering the power output. This would not be sensible since the motivation for smoothing the HRR is to allow higher engine loads. Second, regions with low ϕ may not reach a peak combustion temperature of 1500 K, which is required for complete combustion (see Ref. [29] and Appendix B). A better approach is to combine a well-mixed charge (with ϕ sufficiently high for complete combustion) with a range of ϕ created by late injection [33]. The well-mixed "background" charge can be created by the use of early fuel injection, as illustrated by the SOI = 40°CA case in Fig. 14 (adapted from Ref. [30]). Alternatively, external fuel/air mixing can be used, and this is the approach taken in this work. The fuel stratification is created by injecting a part of the fuel later in the cycle, but well before the combustion event. Figure 14 also demonstrates a typical fuel distribution for injection at 320°CA, using PLIF imaging at 365°CA. This image timing corresponds well to the timing of the combustion event in the current study. However, it should be noted that this previous imaging study used iso-octane fuel [30]. No evidence of the individual sprays can be seen in the right-hand image in Fig. 15. Instead, by 365°CA the fuel has formed a "cloud" that is located near the center of the combustion chamber. This cloud has a range of fuel concentrations, with a tendency for progressively leaner zones on its periphery.

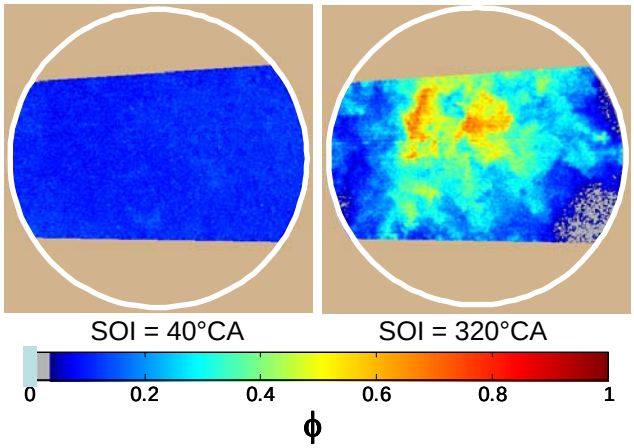

Figure 14. Example of in-cylinder fuel distribution for early and late direct injection using 6-hole injector. PLIF imaging at 365°CA, using iso-octane with overall ϕ = 0.12. Adapted from Ref. [30]. The white circle around each image shows the 70 mm diameter field of view through the piston-crown window.

When attempting to create a staged autoignition event with ethanol, it is important to recall that it is not the ϕ -variations *per se* that are important. Rather, uneven vaporization cooling is the important effect as it is used to enhance the in-cylinder thermal stratification and in this way exploit the high thermal sensitivity of ethanol (Fig. 3a) to create a staged autoignition event.

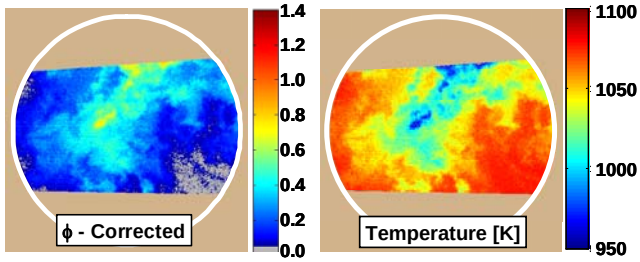

Figure 15. Temperature-corrected ϕ-map, and temperature map at 365°CA, using iso-octane with overall ϕ = 0.12. Reproduced from Ref. [30]. Hollow-cone injector with SOI = 305°CA.

For illustrative purposes, Fig. 15 shows the correlation between the fuel stratification and temperature for iso-octane, which was examined in a previous work [30]. An inverse correlation between the fuel concentration and the temperature can be seen, with the lowest temperatures in the center of

the fuel cloud. The temperature field was computed based on the thermodynamic properties of fuel and air, accounting for vaporization cooling at the time of injection, adiabatic mixing, and subsequent compression heating. These calculations assumed an otherwise uniform temperature field. However, the actual in-cylinder thermal field is more complex because heat transfer and in-cylinder convection are also creating in-cylinder thermal stratification at the same time.

The KIVA-3V CFD results in Fig. 16 demonstrate the thermal field caused by heat transfer [31]. With a RANS turbulence model, the model shows the ensemble-averaged temperature distribution caused by heat transfer. Statistically, the highest in-cylinder temperatures are found in the center of the combustion chamber, as could be expected. By comparing Figs. 14, 15 and 16, it can be realized that heat transfer and vaporization cooling may counteract each other. This could occur because late injection often places the fuel in the center of the combustion chamber, so most vaporization cooling is expected in the regions which normally are the least cooled by heat transfer. Hence, vaporization cooling could potentially reduce the in-cylinder thermal stratification and actually create a faster combustion event, depending on injection timing and other factors. However, it has to be pointed out that the actual thermal field caused by heat transfer is not as smooth as the RANS-based results in Fig. 16 indicate. An example of measured temperature distribution of a single cycle is shown in Fig. 17. The planar imaging of temperature was conducted in the corresponding optical HCCI engine [32]. As can be seen, the in-cylinder charge shows substantial thermal stratification but the structure is very different from the RANS-based model. Instead of a smooth temperature field, hot and cold regions with steep temperature gradients can be observed. As explained in Ref. [32], the locations and shapes of these structures vary from cycle to cycle in a seemingly random fashion. Nonetheless, the magnitude of the thermal stratification remains similar for all cycles. Also, Ref. [32] shows that the thermal stratification develops at an increasing rate during the compression stroke as the temperature difference between the walls and the gas increases due to compression heating.

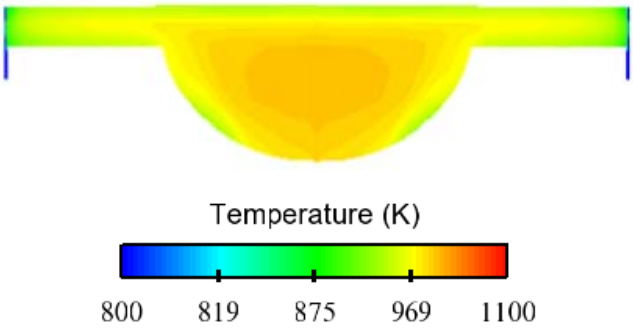

Figure 16. KIVA computations showing a cross-section of the in-cylinder thermal field at 355°CA, just before onset of combustion. No vaporization cooling - premixed ethanol with overall ϕ = 0.40 [31].

In summary, the developing thermal fields due to either heat transfer or fuel/air mixing resulting from late injection are complex by themselves, and it is impossible to estimate how they may interact. Thus, it is not obvious that the application of partial fuel stratification will work as well as the arguments above suggest (*i.e.* Figs. 12 and 14).

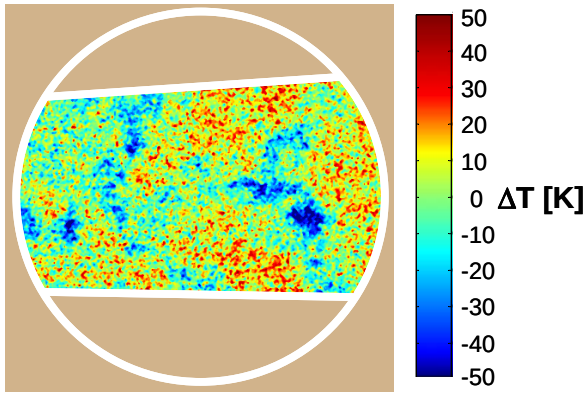

Figure 17. PLIF-based temperature-map at 355°CA in the mid plane of the pancake combustion chamber. Reproduced from Ref. [32].

On a final note, the term “partial fuel stratification” was introduced in earlier work [33] to distinguish the combination of a uniform “background” fuel distribution (using external premixing or early injection) and a stratified fuel distribution (using late injection) from conventional fuel stratification where fuel-free air-only zones are created. This earlier work used partial fuel stratification with two-stage ignition fuels to smooth the HCCI heat release, utilizing the chemistry-based ϕ-sensitivity of these reactive fuels. In the Discussion section below, the current use of partial fuel stratification with ethanol to create thermal stratification is contrasted with this previous study and other more recent studies that used both regular gasoline and more reactive fuels.

SMOOTHING HRR USING PARTIAL FUEL STRATIFICATION

As mentioned in the Introduction, the combustion phasing influences the combustion rate strongly for fully premixed HCCI operation. Specifically, by retarding the combustion phasing a lower peak heat-release rate can be achieved [1,2]. Therefore, it is important to maintain a constant combustion phasing when evaluating the potential of any technique to lower the peak HRR. In this study of partial fuel stratification, it was decided to maintain CA50 fixed at 366°CA. Figure 18 shows how T_{in} had to be adjusted as the fuel injection timing and DI fraction were varied. Fully premixed operation required the lowest T_{in} (148°C) because with the use of the external fuel vaporizer, no heat for fuel vaporization is taken from the in-cylinder air. Conversely, the highest T_{in} for each SOI is required for the 40% case, which has the highest fraction of fuel supplied by direct injection. To first order, the increase in T_{in} above 148°CA is proportional to the DI fraction. For the 20% and 40% DI cases, the highest T_{in} is required for SOI in the 240 – 270°CA range. This suggests that the strongest reduction of the near-TDC temperatures (which

determine the ignition timing) as a result of vaporization cooling occurs for injection around the middle of the compression stroke.

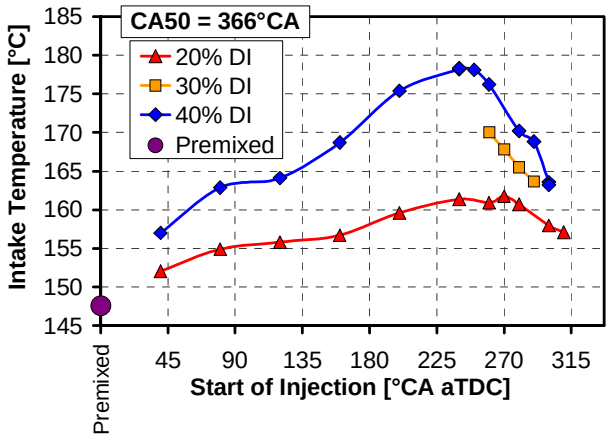

Figure 18. T_{in} required to maintain CA50 = 366°CA for operation with partial fuel stratification. 37.3 mg ethanol/cycle. 1200 rpm, and P_{in} = 100 kPa.

For these tests, it was decided to maintain the ethanol fueling rate constant at 37.3 mg/cycle for all DI fractions and SOIs. This fueling rate corresponds to a supplied ϕ = 0.42 for well-mixed operation with SOI = 40°CA, as shown in Fig. 19. Operation with this early injection required an air-supply rate of 0.801 g/cycle. However, for SOI > 120°CA, the required increase of T_{in} led to a reduction of the inducted gas mass since P_{in} was maintained at 100 kPa. Therefore, Fig. 19 shows that the supplied ϕ rises above 0.42 for the later SOIs since the fueling rate was held constant. The reduced air-mass flow for injection during the compression stroke is a drawback since it reduces the overall dilution level and makes it harder to achieve high loads with acceptable HRR.

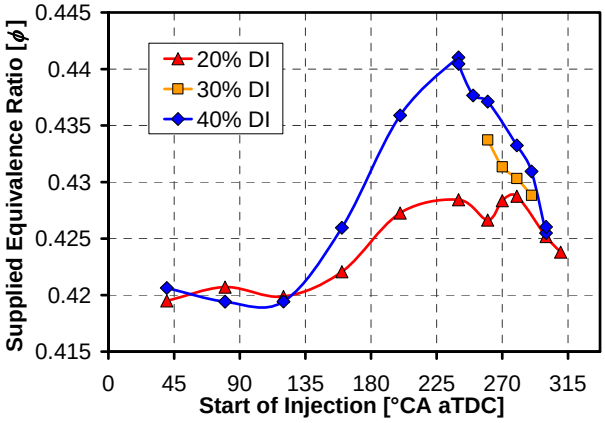

Figure 19. Supplied ϕ for operation with partial fuel stratification. 37.3 mg ethanol/cycle.

Figure 20 plots the 10 – 90% burn duration as a function of SOI for the various DI fractions. It can be seen that the use of partial fuel stratification has a strong influence. For well-mixed operation with SOI = 40°CA, the burn duration is relatively short at 3.5°CA. This corresponds to a relatively high PRR_{max} of 9.7 bar/°CA, as plotted in Fig. 21. The longest burn duration of 5.4°CA is achieved for SOI = 280°CA with a DI fraction of 40%. This operating point has a PRR_{max} of 6.0 bar/°CA. Hence, the application of partial fuel stratification has rendered the desired results with an increase of the burn duration by 55% and a reduction of the PRR_{max} by 39%. These improvements are realized despite the fact that the supplied ϕ increases by 3% due to the increased T_{in}.

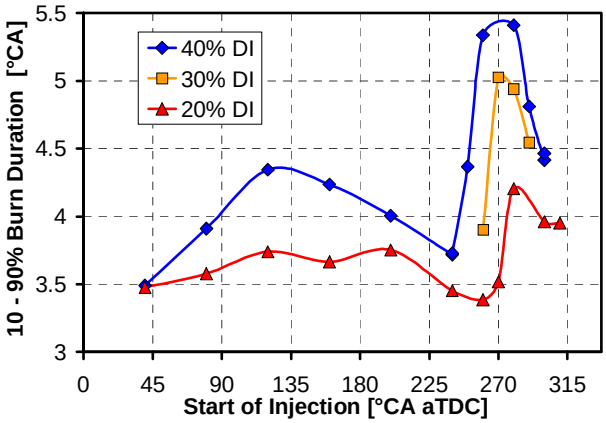

Figure 20. Burn duration for operation with partial fuel stratification using ethanol.

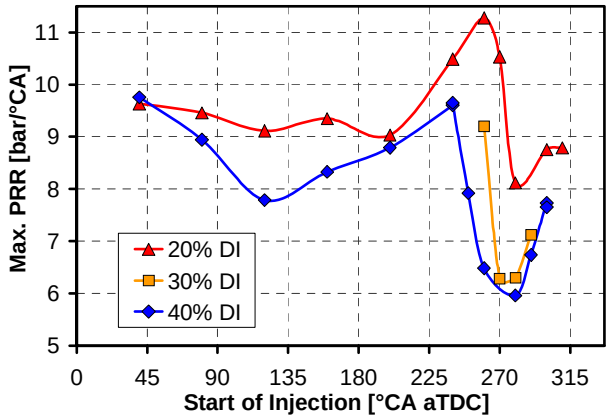

Figure 21. PRR_{max} for operation with partial fuel stratification using ethanol.

An examination of Fig. 20 and 21 shows that the response of the HCCI combustion to the application of partial fuel stratification is complex. This was expected based on the anticipated intricate interactions between fuel/air-mixing and heat transfer, as discussed in the previous section. The operating point with SOI = 260°CA and 20% DI fraction stands out with the highest observed PRR_{max} (11.3 bar/°CA) and the shortest burn duration (3.4°CA). Apparently, the fuel distribution is such that the vaporization-cooled regions partly counteract the developing thermal stratification caused by wall heat transfer. The net result is that a substantial part of the in-cylinder charge becomes more thermally uniform compared to fully premixed operation. With less thermal stratification, both the HRR and PRR increase. Contributing to the higher PRR is a 1.6% increase of the supplied ϕ due to the higher required T_{in}, see Figs. 18 and 19.

Operation with SOI = 280°CA offers the strongest effect of partial fuel stratification, as Figs. 20 and 21 show. Therefore, this SOI is examined to provide

detailed insights into the successful application of partial fuel stratification. Figure 22 shows the HRR, PRR, and pressure for operation with 20, 30 and 40% DI. For reference, well-mixed operation with an early SOI of 40°CA is included. It can be seen that the peak HRR is progressively reduced with increasing DI fraction, consistent with an increasing degree of thermal stratification caused by fuel-vaporization cooling. Also, the combustion has a substantially longer duration for higher DI fractions, with both more early and late heat release. The plots in Fig. 22 are based on the ensemble-averaged pressures traces. Therefore, these plots can potentially be misleading if the amount of cycle-to-cycle variations change with the degree of stratification. Consequently, representative single-cycles were also selected and processed. The statistical selection of single cycles was based on finding cycles with PRR_{max}, CA50, $IMEP_g$, and ringing (knock ripple) very close to the statistical average for each operating point. The result of this process is shown in Fig. 23.

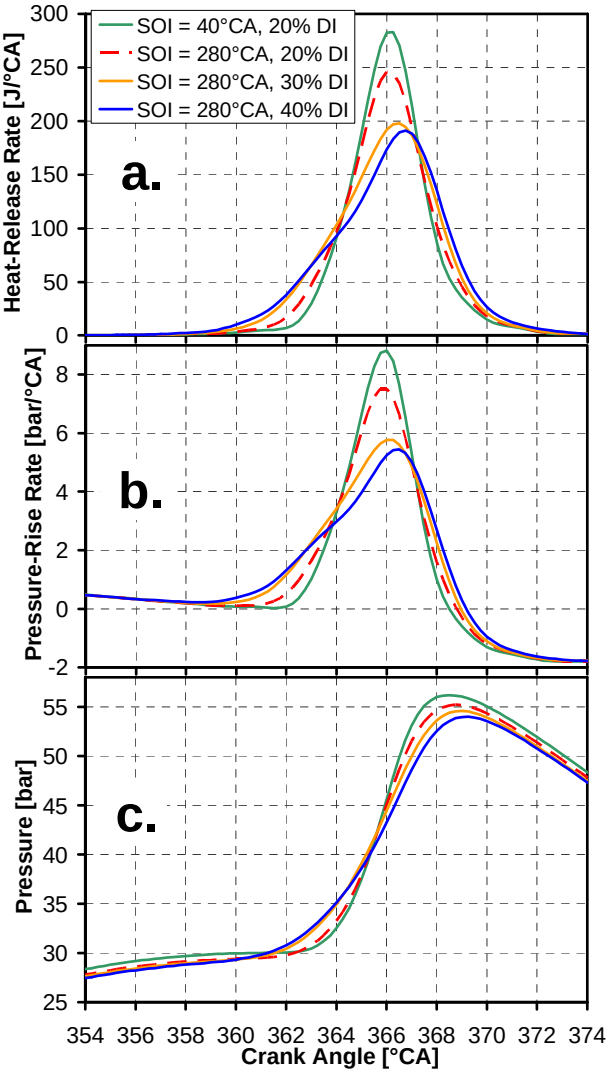

Figure 22. Comparison of operation well-mixed (SOI = 40°CA) and with partial fuel stratification (SOI = 280°CA). HRR (a) and PRR (b) are computed from the ensemble-averaged pressure traces (c). CA50 = 366°CA.

The single-cycle results in Fig. 23 are consistent with the ensemble-averaged results in Fig. 22. For example, Fig. 23a shows a progressively broader heat release with increasing DI fraction, similar to Fig. 22a. In addition, Fig. 23c shows a reduction of the high-frequency ripple on the pressure traces with higher DI fraction. This demonstrates the transition from well-mixed operation with an unacceptably high ringing intensity of 7.1 MW/m^2 to relatively quiet engine operation with a ringing intensity of 2.8 MW/m^2.

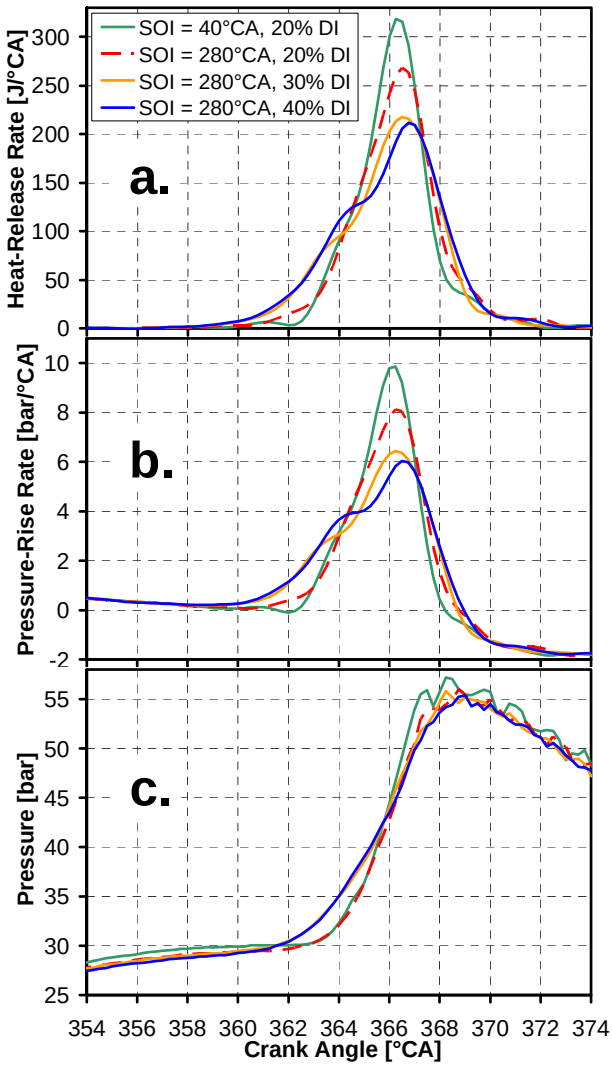

Figure 23. Comparison of operation well-mixed (SOI = 40°CA) and with partial fuel stratification (SOI = 280°CA). HRR (a) and PRR (b) are computed from statistically selected single-cycle pressure traces (c).

Examination of Fig. 23a confirms that the peak HRR is reduced and that the combustion is occurring over a wider range of crank angles, as was observed in the ensemble-averaged results. However, the single-cycle results in Fig. 23a also reveals that the HRR profile changes with the application of partial fuel stratification. Both the 30 and 40% cases show a reduced rise rate of the HRR around 364-365°CA. This feature is even more pronounced when examining the PRR in Fig. 23b. To examine if these unusual HRR and PRR profiles occur frequently, additional single cycles were statistically selected and processed. Figure 24 shows the PRR for the eight cycles that best match both the average PRR_{max} and CA50. Of these cycles, five show this unconventional PRR profile, whereas three have a more traditional

smooth profile. Hence, this indicates that the application of partial fuel stratification has a tendency to produce non-conventional combustion-rate profiles, in addition to its sought-after ability to reduce the peak HRR.

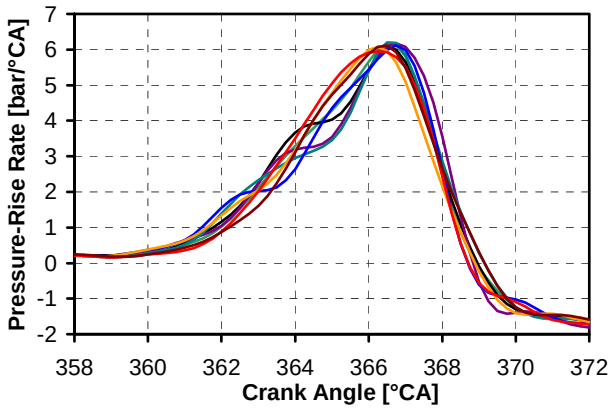

Figure 24. Eight statistically selected single-cycle PRR traces for operation with 40% DI fraction and SOI = 280°CA.

The origin of the unusual combustion-rate profiles leading to the peculiar PRR profiles in Fig. 24 can be traced back to the in-cylinder thermal stratification. To fully understand the detailed nature of this thermal stratification, it would be required to perform either detailed modeling or in-cylinder optical diagnostics. However, the observed HRR and PRR profiles could potentially be explained by the formation a bi-modal statistical distribution of the in-cylinder temperature. An example of a possible temperature distribution is shown in Fig. 25. The "normal" distribution (dashed line) is reproduced directly from KIVA-CFD results in Ref. [34], so it shows the statistical representation of the in-cylinder thermal distribution caused by wall-heat transfer.

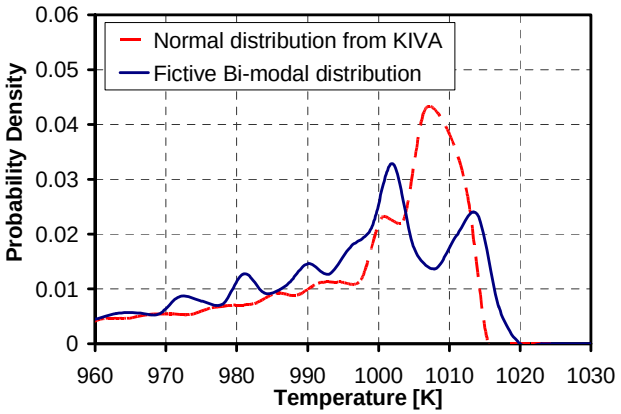

Figure 25 Illustration of potential temperature distributions prior to ignition that could explain the difference between normal and "bi-modal" HRR profiles. The normal distribution is reproduced from KIVA-CFD results in Ref. [34], and is for iso-octane combustion with CR = 18, but with the chemistry turned off.

The KIVA computations are for operation with iso-octane and CR = 18, but with the chemistry turned off to isolate the effects of heat transfer. Therefore, the conditions are not exactly that of the current experiment. Nonetheless, the main feature of the KIVA pdf profile in Fig. 25 is a relatively smooth peak, and this temperature distribution would create a typical HRR profile. In contrast, the solid blue curve represents a fictive temperature distribution which potentially could produce the unusual HRR and PRR profiles in Figs. 23a and 24. In this case, the hottest "bump" around 1014 K would initiate the combustion. The valley around 1008 K would lead to a slowing of the combustion spread in the combustion chamber, corresponding to the less steep portion of the PRR curve around 364-365°CA for 40% DI in Fig. 23b. The combustion spread would then increase again corresponding to the second peak around 1002 K in Fig. 25. This fictive temperature distribution can be related to partial fuel stratification. The hottest peak would correspond to the regions not affected much by heat transfer or by vaporization cooling. The second peak could correspond to regions with significant influence of vaporization cooling and some heat transfer. Finally, the "tail" could correspond to regions that are cooled strongly by heat transfer.

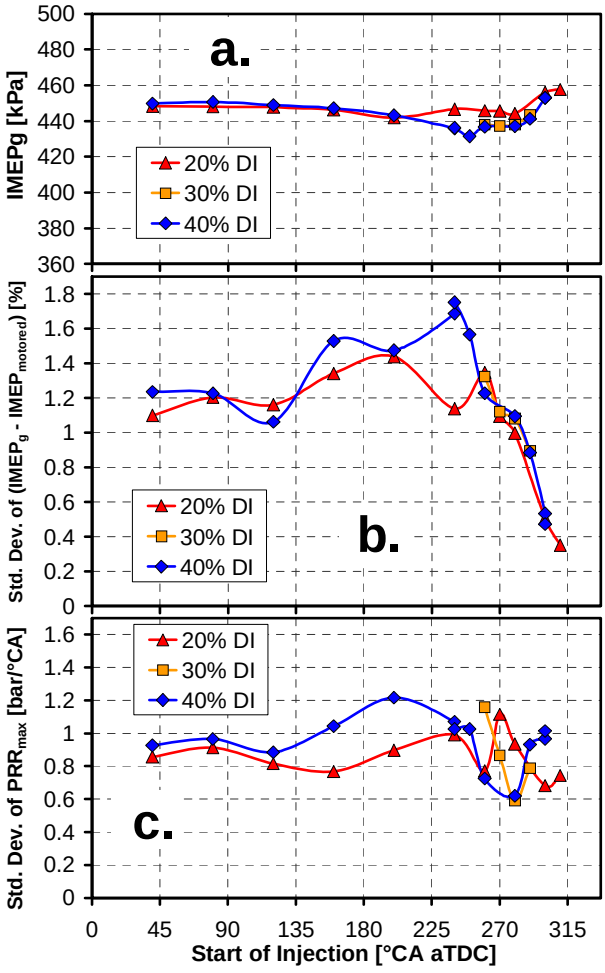

Figure 26. (a) $IMEP_g$, (b) standard deviation of ($IMEP_g$ - $IMEP_{motored}$), and (c) standard deviation of PRR_{max} for operation with partial fuel stratification.

With this discovery of differences in combustion rate between individual cycles it is important to question whether the application of partial fuel stratification renders a combustion system that is sufficiently consistent from cycle to cycle. Some aspects related

to this are plotted in Fig. 26. The $IMEP_g$ includes the compression and expansion strokes, and most points fall in the 435-450 kPa range, as shown in Fig. 26a. Overall, the influence of partial fuel stratification on the $IMEP_g$ is small. Only a minor reduction of $IMEP_g$ is observed for operation with low PRR_{max} using SOI = 280°CA, compared to well-mixed operation using SOI = 40°CA. Figure 26b shows the normalized standard deviation of the $IMEP_g$ *rise* above the motored $IMEP_g$, which is -50 kPa due to normal heat-transfer losses and blow-by[1]. For well-mixed operation, $IMEP_g$ variations are on the order of 1.2%. There are some operating points for SOI in the 160 - 250°CA range with significantly increased $IMEP_g$ variations. However, these are not very important since they do not provide much reduction of the PRR_{max}. For the operating points with the strongest reduction of PRR_{max} (SOI = 280°CA), the $IMEP_g$ variations are similar or slightly lower than for well-mixed operation. Interestingly, the most stable $IMEP_g$ is found for highly stratified operation with late SOI. Furthermore, Fig. 26c shows the standard deviation of PRR_{max}. The lowest variations are found for operation with SOI = 280°CA, indicating that this application of partial fuel stratification consistently maintains a low PRR_{max} for all cycles.

It is also important to maintain low emissions. Figure 27a shows the combustion efficiency computed from the emissions of CO and HC in Fig. 27b. Combustion efficiency remains high for all points, but there is a small but significant drop for operation with low PRR_{max} and SOI around 280°CA. This occurs because the HC emissions are somewhat elevated for these points. Because the HC emission improve for more stratified operation with even later SOI, it is not likely that the elevated HC emission stem directly from overly lean or rich zones created by the fuel stratification. A more credible explanation based on analysis done in Ref. [11] is that HC emissions increase for SOI around 280°CA because the piston position allows the fuel jets to place fuel near the crevice region above the piston rings. A part of this fuel then flows into the ring-land crevice during the compression stroke and contributes to increased HC emissions by escaping the combustion event and then flow out of the crevice during the expansion stroke. This explanation is consistent with an enhanced thermal stratification when the PRR is low. If the fuel jets place the fuel near the crevice, the fuel vaporization cools the regions that also see strong heat transfer, as Fig. 16 shows. In this way, the overall in-cylinder thermal stratification is enhanced.

In addition, a part of the increased HC emissions could be related to the observed reduction of PRR for SOI near 280°CA. Analysis of the data shows a fair correlation between reduced PRR_{max} and increased HC. As discussed in Ref. [6], with a low PRR the combustion-induced compression heating of the coldest and not-yet-ignited zones of the in-cylinder charge can become so weak that the hot-ignition temperature is never reached in these zones. In this way, operation with reduced PRR_{max} can cause the near-wall regions to increase their contribution to the HC emissions.

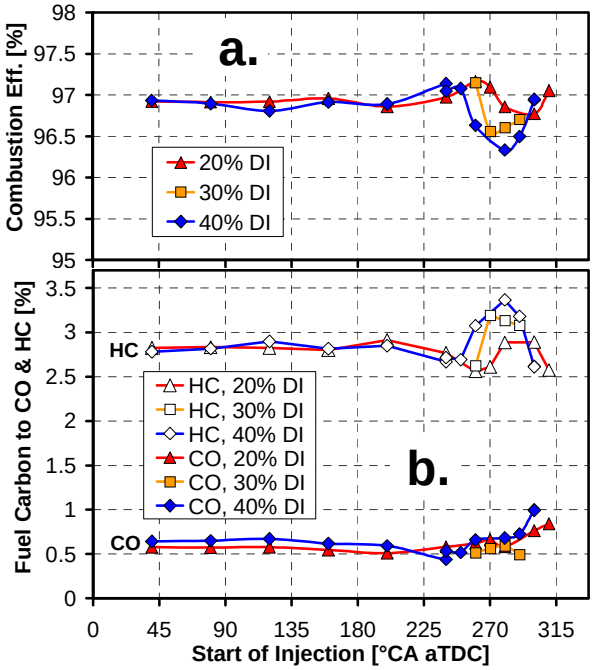

Figure 27. (a) Combustion efficiency, (b) CO and HC exhaust emissions for operation with partial fuel stratification.

CO emissions have a different formation pathway [11] and do not correlate with PRR_{max}. In fact, the CO emissions are very low for all operating points. Nonetheless, a slight tendency for increased CO emissions can be detected for the most stratified operation with late SOI. This small increase of CO could be caused by the creation of leaner-than-average zones in the near-wall regions. However, since at least 60% of the fuel is supplied fully premixed, the lowest possible in-cylinder ϕ is around 0.25, which normally burns to completion for this relatively advanced CA50 = 366°CA. With the use of a DI fraction higher than 40%, increased CO is likely to become an issue for late SOIs, as the lowest in-cylinder ϕ then can cause bulk-gas contributions to the CO emissions [9].

With the use of fuel stratification in HCCI-type engines, it is important to monitor the NO_x emissions [30,35]. Figure 28 shows the indicated specific NO_x emissions for this study using partial fuel stratification. It is clear that unacceptable NO_x can be produced easily if too much stratification is applied, and the points for the latest SOIs fall above the plot area. Fortunately, for operation with low PRR_{max} using SOI = 280°CA the NO_x emissions are relatively low and fall below the US2010 limit for heavy-duty engines, which is 0.27 g/kWh. It is interesting that the 20% and 40% cases show local NO_x maxima for operation with SOI in the 240-260°CA range, despite the lower degree of fuel stratification compared to operation with SOI = 280°CA. However, these maxima correspond to the higher supplied ϕ for these SOI, as

[1] The relative combustion instability is evaluated based on the increase of $IMEP_g$ above the motored $IMEP_g$ in order to be able to use the same equations to consistently evaluate the normalized standard deviation also for low-load operation with $IMEP_g$ near or below zero.

shown in Fig. 19, and discussed in conjunction with Fig. 18. The NO_x emissions have a high sensitivity to changes of the supplied ϕ because the combination of fueling rate and selected CA50 is fairly aggressive with mass-averaged peak-combustion temperatures near 1950 K, even for well-mixed operation. Hence, a significant amount of NO_x is formed even for well-mixed operation with SOI = 40°CA. It is interesting that operation with 40% DI and SOI = 120°CA leads to a global minimum of the NO_x emissions despite that some degree of stratification is increasing the burn duration and reducing the PRR_{max}, as shown in Figs. 20 and 21. From this perspective, partial fuel stratification using SOI = 120°CA could be a good option when NO_x emissions need to be minimized and only a modest degree of PRR_{max} reduction is required.

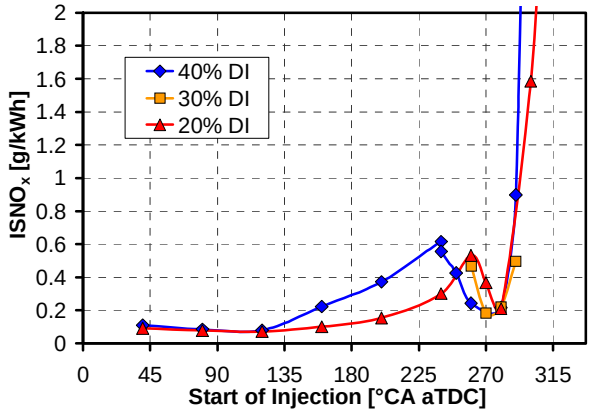

Figure 28. Indicated specific NO_x exhaust emissions for operation with partial fuel stratification.

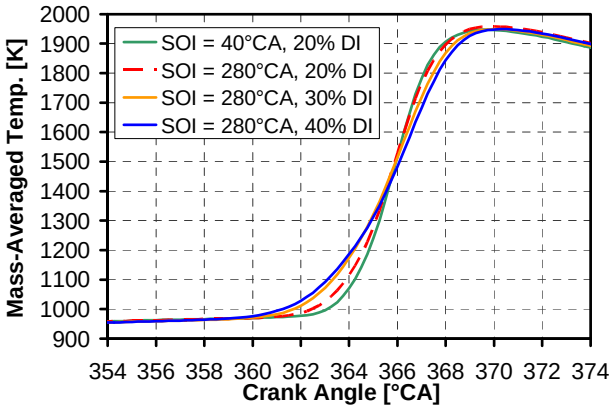

Figure 29. Mass-averaged temperature traces computed from the ensemble-averaged pressure traces for operation well-mixed (SOI = 40°CA) and with partial fuel stratification (SOI = 280°CA).

Temperature traces, as determined by analysis of the in-cylinder pressure, are plotted in Fig. 29 for both well-mixed operation and for operation with partial fuel stratification using SOI = 280°CA. As mentioned above, the mass-averaged peak-combustion temperature is near 1950 K for the well-mixed case. Perhaps surprisingly, the peak temperatures barely change with stratification level. However, the local peak combustion temperature must increase for the partially stratified cases since their NO_x emissions are higher than the well-mixed operating point, as shown in Fig. 28. Furthermore, it can be observed that the mass-averaged temperatures prior to onset of combustion are very similar, regardless of the degree of fuel stratification. This may also be somewhat surprising given the large differences in T_{in} together with substantial variations in the supplied ϕ, as shown in Fig. 19.

DISCUSSION

In this study, it has been demonstrated that partial fuel stratification with ethanol can be used to create vaporization-cooling-induced thermal stratification, and in this way reduce the peak HRR. As mentioned above, the term “partial fuel stratification” was introduced in earlier work using two-stage ignition fuels, see Ref. [33]. Recent follow-up studies have demonstrated a strong reduction of the peak HRR through the use of partial fuel stratification with reactive low-octane fuels like PRF73 [36] and a selected petroleum distillate [37]. Hence, both a high-octane single-stage ignition fuel like ethanol and low-octane two-stage ignition fuels can be used to create a staged combustion event and reduce the peak HRR. However, there are fundamental differences in how this staged combustion event is accomplished for the various fuels.

In the current study using ethanol, the first autoignition events occur in the leanest zones because these have experienced the least amount of vaporization cooling and they also have the highest γ. The sequential autoignition then progresses from leaner (hotter) to richer (colder) zones, driven by the compression heating associated with the pressure rise from the already burned zones. The fuel used, ethanol, has very low ITHR so the rate of progress from leaner to richer zones is primarily controlled by the thermal stratification, in particular since the autoignition timing of ethanol is sensitive to temperature variations (see Fig. 3a).

A contrasting second scenario is when reactive two-stage fuels are used together with partial fuel stratification. In this case, the first autoignition occurs in the richest zones because these zones have both more LTHR and ITHR compared to the leaner zones. The influence of vaporization cooling is small, partly because the AFR is higher and the heat of vaporization is less than for ethanol, and partly because the ignition timing of these fuels is relatively insensitive to variations of the temperature (see Fig. 3b). The sequential autoignition then progresses from richer to leaner zones, driven partly by the already proceeding autoignition reactions (which were initiated during the LTHR), and partly by the compression heating associated with the pressure rise from the already burned zones.

A third scenario is the use of partial fuel stratification with a single-stage ignition fuel that does not have strong vaporization cooling, nor much enhancement of the autoignition chemistry (ITHR) with increasing ϕ. It was demonstrated in both Refs. [36] and [38] that

such a fuel does not lead to a reduction of the peak HRR when partial fuel stratification is applied. The tested fuels were iso-octane and gasoline, both under naturally aspirated conditions with P_{in} = 100 kPa.

However, a fourth scenario can develop when the intake pressure is increased, as recently demonstrated for gasoline by Dec *et al.* [38]. Under boosted conditions gasoline starts exhibiting enhanced ITHR and develops a strongly negative ϕ-sensitivity (*i.e.* richer regions autoignite before the leaner regions). Under these conditions, partial fuel stratification becomes effective for reducing the peak HRR, even for a fuel that still does not show LTHR.

TABLE 4. Comparison of Fuel Effects for Partial Fuel Stratification

Scenario #:	**1**	**2**	**3**	**4**
Fuel and P_{in}: : Effect or : Property	**Ethanol P_{in} = 100 kPa**	**PRF73 P_{in} = 100 kPa**	**Gasoline P_{in} = 100 kPa**	**Gasoline P_{in} = 200 kPa**
Demonstrated HRR Reduction with Partial Fuel Stratification	Large	Very Large	None	Very Large
Dominating Sequential Autoignition Process	Lean to Rich	Rich to Lean	Hot to Cold	Rich to Lean
Vaporization Cooling	Strong	Weak	Weak	Weak
LTHR	No	Yes	No	No
ITHR	Very Weak	Strong	Weak	Strong
Temperature Sensitivity	High	Very Low	High	Low
Sensitivity of Autoignition Chemistry to Changes of ϕ	Very Low	High	Low	High
δCA10/$\delta\phi$ for Direct Injection	Highly Pos-itive	Highly Neg-ative	Near Zero	Highly Neg-ative

In summary, the use of ethanol to create a staged autoignition is one out of three distinct scenarios where partial fuel stratification is applied successfully. The most important features of these are summarized in Table 4. Of critical importance to the use of partial fuel stratification is that the autoignition timing is sensitive to changes of the local ϕ when direct injection is used. This sensitivity needs to be either highly positive (ethanol) or highly negative (reactive fuels), as indicated in the bottom row of Table 4. Note that the use of partial fuel stratification with gasoline at P_{in} = 100 kPa did not provide a reduction of the peak HRR, but this scenario #3 is included for completeness.

CONCLUSIONS

For a given engine load, ethanol's high latent heat of vaporization in combination with its low stoichiometric air/fuel ratio results in very strong in-cylinder vaporization cooling compared to gasoline.

Ethanol has true single-stage ignition characteristics with only minor enhancement of the autoignition reactivity with increasing ϕ. Therefore, the autoignition timing is sensitive to variations of the charge temperature.

With the application of partial fuel stratification using a combination of premixed fueling and late direct injection, considerable enhancement of the in-cylinder thermal stratification was accomplished. This was evidenced by a large increase of the burn duration and a strong reduction of the peak HRR. The current experiments using a multi-hole injector show that a combination of 60 – 70% premixed charge and injection of 30 – 40 % of the fuel at 60°CA before TDC is most effective for smoothing the HRR. With CA50 held fixed, this increases the burn duration by 55% and reduces the maximum pressure-rise rate by 40%.

A large fraction of the cycles show a typical broadened HRR profile, but roughly half of the cycles have an unusual shape of the HRR profile, suggesting the formation of a bi-modal thermal distribution in the combustion chamber. Nonetheless, the $IMEP_g$ and PRR_{max} both exhibit low cyclic variability, indicating a stable combustion process despite the cycle-to-cycle variations of the HRR profile.

Both the developing thermal field caused by normal heat transfer and the ongoing fuel/air mixing caused by late direct injection of fuel are complex by themselves, and it is impossible to estimate how they interact. With better understanding of these in-cylinder processes through modeling and optical diagnostics, it is likely that the experiment can be tailored to achieve substantially stronger reduction of the peak HRR than demonstrated here.

ACKNOWLEDGEMENTS

The authors would like to thank Paul Najt of General Motors for valuable discussions leading up to this work. Thanks also to Yi Yang for discussions and insights regarding the application of partial fuel stratification for two-stage ignition fuels, and to Richard Steeper for constructive suggestions on the

manuscript. Finally, many thanks go to Kenneth St. Hilaire, Dave Cicone, Chris Carlen, and Gary Hubbard for their dedicated support of the HCCI laboratory.

The work was performed at the Combustion Research Facility, Sandia National Laboratories, Livermore, CA. Financial support was provided by the U.S. Department of Energy, Office of Vehicle Technologies. Sandia is a multiprogram laboratory operated by the Sandia Corporation, a Lockheed Martin Company, for the United States Department of Energy's National Nuclear Security Administration under contract DE-AC04-94AL85000.

REFERENCES

1. Sjöberg, M., Dec, J.E., and Cernansky, N.P., "Potential of Thermal Stratification and Combustion Retard for Reducing Pressure-Rise Rates in HCCI Engines, based on Multi-Zone Modeling and Experiments," SAE Technical Paper 2005-01-0113, 2005.
2. Olsson, J.-O., Tunestål, P., Johansson, B., Fiveland, S., Agama, J.R., and Assanis, D.N., "Compression Ratio Influence on Maximum Load of a Natural Gas-Fueled HCCI Engine", SAE Paper 2002-01-0111, 2002.
3. Sjöberg, M. and Dec, J.E., "Comparing Late-cycle Autoignition Stability for Single- and Two-Stage Ignition Fuels in HCCI Engines," Proceedings of the Combustion Institute, 31: 2895–2902, 2007.
4. Dec, J.E. and Yang, Yi, "Boosted HCCI for High Power without Engine Knock and with Ultra-Low NOx Emissions – using Conventional Gasoline," SAE Technical Paper 2010-01-1086.
5. Christie, M.J., Fortino, N., and Yilmaz H., "Parameter Optimization of a Turbo Charged Direct Injection Flex Fuel SI Engine," SAE Technical Paper 2009-01-0238, 2009.
6. Sjöberg, M. and Dec, J.E., "Ethanol Autoignition Characteristics and HCCI Performance for Wide Ranges of Engine Speed, Load and Boost," SAE Technical Paper 2010-01-0338, 2010
7. US Environmental Protection Agency, http://www.epa.gov/otaq/fuels/renewablefuels/index.htm .
8. Sjöberg, M. and Dec, J. E. "Effects of Engine Speed, Fueling Rate, and Combustion Phasing on the Thermal Stratification Required to Limit HCCI Knocking Intensity," *SAE Transactions*, Vol. 114, Sec. 3, pp. 1472-1486, SAE paper no. 2005-01-2125, 2005.
9. Dec, J.E. and Sjöberg, M., "A Parametric Study of HCCI Combustion – the Sources of Emissions at Low Loads and the Effects of GDI Fuel Injection," SAE Technical Paper 2003-01-0752, 2003.
10. Heywood, J.B., "Internal Combustion Engine Funda-mentals," McGraw-Hill, New York, ISBN 13: 9780070286375, 1988.
11. Dec, J.E, Davisson, M.L., Sjöberg, M., Leif, R.N., and Hwang, W., "Detailed HCCI Exhaust Speciation and the Sources of Hydrocarbon and Oxygenated Hydrocarbon Emissions," SAE Technical Paper 2008-01-0053, 2008.
12. Sjöberg, M. and Dec, J.E., "Effects of EGR and Its Constituents on HCCI Autoignition of Ethanol," Proceedings of the Combustion Institute, Vol. 33, pp. 3031-3038, 2011. DOI: 10.1016/j.proci.2010.06.043.
13. Lutz, A. E., Kee, R. J., and Miller, J. A., "Senkin: A FORTRAN Program for Predicting Homogeneous Gas Phase Chemical Kinetics with Sensitivity Analysis," Sandia National Laboratories Report No. SAND87-8248.
14. Lutz, A.E., "Multi-zone Model for Homogeneous Ignition," Sandia National Laboratories, Internal Report, July 8, 2002.
15. Curran H., Serinyel, Z., and Metcalfe, W., Combustion Chemistry Centre at NUI Galway, Ireland, personal communication, 2010.
16. Mehl, M., Pitz, W.J., Sjöberg, M., and Dec, J.E., "Detailed Kinetic Modeling of Low-Temperature Heat Release for PRF Fuels in an HCCI Engine," SAE Technical Paper 2009-01-1806, 2009.
17 Marinov, N.M., "A Detailed Chemical Kinetic Model for High Temperature Ethanol Oxidation," *International Journal of Chemical Kinetics.* Vol 31, Issue 3, pp. 183-220, 1999. DOI: 10.1002/(SICI)1097-4601(1999)31:3<183::AID-KIN3>3.0.CO;2-X.
18 Li, J., Kazakov, A., Chaos, M., and Dryer, F.L., "Chemical Kinetics of Ethanol Oxidation," Paper C26, 5th US Combustion Meeting, San Diego, 2007.
19. Hawkes, E., University of New South Wales, Australia, personal communication, 2010.
20. Hwang, W., Dec, J.E., and Sjöberg, M., "Spectroscopic and Chemical-Kinetic Analysis of the Phases of HCCI Autoignition and Combustion for Single- and Two-Stage Ignition Fuels", Combustion and Flame, 154(3), pp. 387-409, 2008.
21. Konno, M., Chen, Z., and Miki, K., "Computational and Experimental Study on the Influence of Formaldehyde on HCCI Combustion Fueled with Dimethyl Ether", JSAE Technical Paper 20030283 (SAE 2003-01-1826), 2003.
22. Yamaya, Y., Furutani, M., and Ohta, Y., "Premixed compression ignition of formaldehyde-doped lean butane/air mixtures in a wide range of temperature", SAE Paper 2004-01-1977, 2004.
23. Grandin, B., Denbratt, I., Bood, J., Brackmann, C., Bengtsson, P.-E., "A Study of the influence of exhaust gas recirculation and stoichiometry on the heat release in the end-gas prior to knock using rotational coherent anti-Stokes Raman spectroscopy thermometry," *Int. J. of Engine Research* **3**(4):209-221, 2002.
24. NIST Chemistry WebBook, "Standard Reference Database Number 69," March 2009, http://webbook.nist.gov/chemistry/
25. Flowers, D.L., Aceves, S.M., Martinez Frias, J., "Improving Ethanol Life Cycle Energy Efficiency by Direct Utilization of Wet Ethanol in HCCI Engines", JSAE Technical Paper 20077037 (SAE 2007-01-1867), 2007.

26. Dec, J.E. and Sjöberg, M., “Isolating the Effects of Fuel Chemistry on Combustion Phasing in an HCCI Engine and the Potential of Fuel Stratification for Ignition Control,” SAE Technical Paper 2004-01-0557, 2004.
27. Sjöberg, M. and Dec, J.E., “An Investigation of the Relationship between Measured Intake Temperature, BDC Temperature, and Combustion Phasing for Premixed and DI HCCI Engines,” SAE Technical Paper 2004-01-1900, 2004.
28. Anderson, R.W., Yang, J., Brehob, D.D., Vallance, J.K., and Whiteaker, R.M., "Understanding the Thermodynamics of Direct-Injection Spark-Ignition (DISI) Combustion Systems: An Analytical and Experimental Investigation", SAE paper 962018.
29. Sjöberg, M. and Dec, J. E., “An investigation into lowest acceptable combustion temperatures for hydrocarbon fuels in HCCI engines,” *Proceedings of the Combustion Institute* **30**:2719 – 2726, 2005.
30. Hwang, W., Dec, J. E., and Sjöberg, M. (2007), “Fuel Stratification for Low-Load HCCI Combustion: Performance and Fuel-PLIF Measurements, *SAE Transactions* 116(3), pp. 1437-1460, paper 2007-01-4130.
31. Brakora, J., Engine Research Center at University of Wisconsin – Madison, personal communication, 2010.
32. Dec, J.E., and Hwang, W., ”Characterizing the Development of Thermal Stratification in an HCCI Engine Using Planar-Imaging Thermometry,” SAE Technical Paper 2009-01-0650, 2009.
33. Sjöberg, M. and Dec, J.E., “Smoothing HCCI Heat-Release Rates using Partial Fuel Stratification with Two-Stage Ignition Fuels”, SAE Paper 2006-01-0629, 2006.
34. Sjöberg, M., Dec, J.E., Babajimopoulos, A., and Assanis, D., “Comparing Enhanced Natural Thermal Stratification against Retarded Combustion Phasing for Smoothing of HCCI Heat-Release Rates,” SAE Technical Paper 2004-01-2994, 2004.
35. De Zilwa, S. and Steeper, R., “Predicting NO_x Emissions from HCCI Engines Using LIF Imaging,” SAE paper 2006-01-0025, 2006.
36. Yang, Y., Dronniou, N., Sjöberg, M., and Dec, J.E., “Tailoring HCCI Heat Release Rates with Partial Fuel Stratification: Comparison of Two-Stage and Single-Stage Ignition Fuels”, Proceedings of the Combustion Institute Vol. 33 (2011), pp. 3047-3055 DOI: 10.1016/j.proci.2010.06.114.
37. Yang, Y., Dronniou, N., Sjöberg, M., and Dec, J.E., “Partial Fuel Stratification to Control HCCI Heat Release Rates: Fuel Composition and Other Factors Affecting Pre-Ignition Reactions of Two-Stage Ignition Fuels”, SAE Paper 2011-01-1359, 2011.
38. Dec, J.E., Yang, Y., and Dronniou, N., “Boosted HCCI – Controlling Pressure-Rise Rates for Performance Improvements using Partial Fuel Stratification with Conventional Gasoline”, SAE Paper 2011-01-0897, 2011.

APPENDIX A: THERMAL DISTRIBUTION FOR MULTI-ZONE MODEL

The purpose of the multi-zone modeling presented in the main body of the paper is to predict how the start of combustion (CA10) responds to changes of ϕ. For these predictions, it is not critical to capture correctly the heat-release rate during the full combustion event. Therefore, a single-zone model could have been used. Nonetheless, since a multi-zone model was available and configured based on recent work in Ref. [6] it was also used for this study. The pressure-rise rate during combustion is made to approximate that of the experiment by initializing the ten active zones with different temperatures, for a total thermal width (TW) of 25K at BDC, as illustrated in Fig. A1. To make the total pressure rise during combustion better match that of the experiment, the 11th “inactive” zone is initialized sufficient cold at BDC so that it never ignites. This zone represents 16% of the total in-cylinder mass, as illustrated in Fig. A1. These 16% account for combustion inefficiencies and heat-transfer (and to a lesser extent blow-by) on the pressure rise during combustion. The inactive zone is needed since the model is adiabatic and does not include heat-transfer.

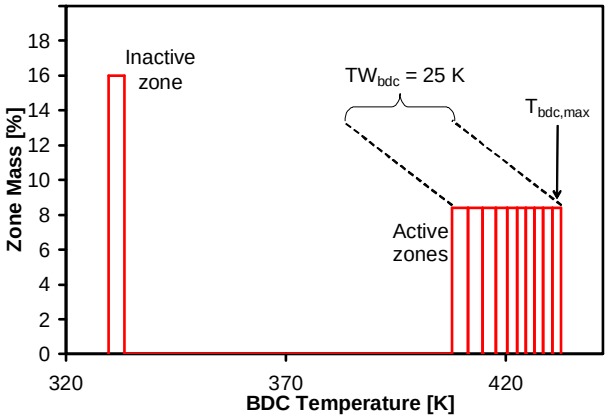

Figure A1. Illustration of the zone distribution used for the 11-zone model.

Figure A2 shows that the chosen temperature distribution makes the pressure during combustion match the experiment very well for the more advanced combustion phasing. Also the more retarded case in Fig. B2 has a good pressure match until well past the CA10 point of 369.2°CA. Hence, the chosen thermal distribution should serve very well for capturing the timing of CA10, and probably also for CA50. A more detailed description of the model setup can be found in Ref. [6].

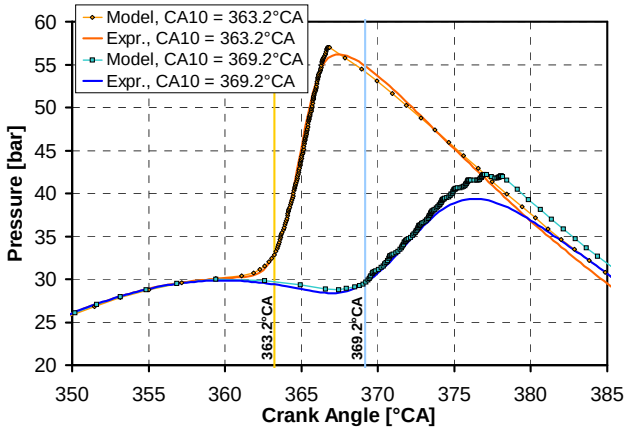

Figure A2. Comparison of pressure traces for the model and fully premixed experiment using ethanol. ϕ = 0.40, 1200 rpm, and P_{in} = 100 kPa.

APPENDIX B: REQUIRED TEMPERATURE FOR COMPLETE COMBUSTION OF ETHANOL

One of the beneficial features of HCCI combustion is that very lean and/or dilute charge can be ignited and burned. However, to ensure low exhaust emissions and high thermal efficiency, it is not sufficient to ensure that ignition has occurred throughout the fuel/air charge, but also that the combustion proceeds to completion. Incomplete combustion is a particular concern for low-load operation, but also when fuel stratification is used for moderate and high loads [9]. The onset of combustion incompleteness varies greatly with both fuel type and operating conditions. However, for a given engine speed, the requirement for complete combustion can be summarized by the need to reach a minimum peak-combustion temperature. For an engine speed of 1200 rpm, the study in Ref. [29] showed that a wide range of hydrocarbon fuels all burn completely when the a peak temperature of 1500 K is reached. Reaching this temperature allows completion of the last step of the combustion process, namely the CO-to-CO_2 conversion. This holds true regardless of the combination of combustion phasing and ϕ used to reach 1500K. However, the study in Ref [29] did not include any oxygenated fuels like ethanol. Since the conversion of CO to CO_2 is the last combustion step regardless of the relative content of C, H and O atoms, is may be expected that the lowest acceptable combustion temperature is the same for oxygenated fuels. Nevertheless, additional chemical-kinetics modeling was performed to examine this. To be consistent with the modeling in Ref. [29], an identical single-zone model was used but with the current ethanol mechanism [15]. The most important results are shown in Fig. B1.

Most of the data in Fig. B1 are for CR = 18 because a high-CR piston was installed for the experiments that Ref. [29] is based on. Comparing the CO emissions for all fuels at CR = 18, it can be seen that the model predicts that ethanol requires approximately 20 K higher temperatures to reach complete combustion. The reasons for this slight shift is unclear and additional experiments and modeling are needed to confirm this finding.

The current experimental study of ethanol combustion in the main body of this paper uses a CR = 14 piston. Based on this, it was decided to examine the sensitivity of the CO emissions to changes of CR. Figure B1 also includes the ethanol model results for CR = 10. It can be seen that the reduction of CR from 18 to 10 reduces the peak-combustion requirement by roughly 40 K. This shift occurs mainly because with a lower CR the piston-expansion cooling occurs more slowly. This allows more time for the relatively slow CO-to-CO_2 reactions to proceed to completion. Furthermore, the CR = 18 and CR = 10 curves for ethanol bracket the other fuels at low CO levels. This suggests that 1500 K is lowest acceptable combustion temperature for the current experimental study using ethanol with a CR = 14 piston at 1200 rpm.

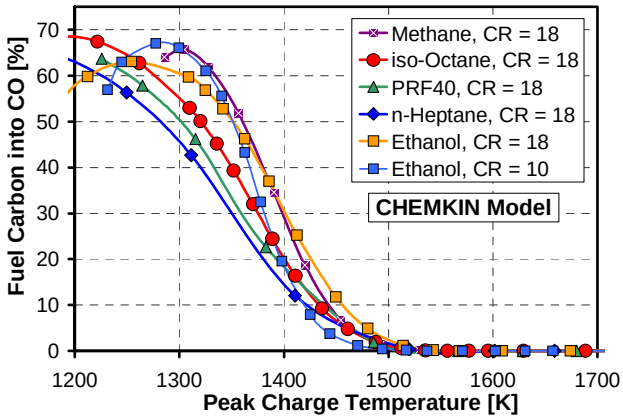

Figure B1. Model results showing correlation between peak combustion temperature and the CO emissions for a range of fuels. 1200 rpm, and P_{in} = 100 kPa.